



## 1 **Molecular composition and volatility of multi-generation** 2 **products formed from isoprene oxidation by nitrate radical**

3 Rongrong Wu<sup>1,2</sup>, Luc Vereecken<sup>1</sup>, Epameinondas Tsiligiannis<sup>3</sup>, Sungah Kang<sup>1</sup>, Sascha R.  
4 Albrecht<sup>1,a</sup>, Luisa Hantschke<sup>1</sup>, Defeng Zhao<sup>4</sup>, Anna Novelli<sup>1</sup>, Hendrik Fuchs<sup>1</sup>, Ralf Tillmann<sup>1</sup>,  
5 Thorsten Hohaus<sup>1</sup>, Philip T.M. Carlsson<sup>1</sup>, Justin Shenolikar<sup>5</sup>, François Bernard<sup>6</sup>, John N.  
6 Crowley<sup>5</sup>, Juliane L. Fry<sup>7</sup>, Bellamy Brownwood<sup>7</sup>, Joel A. Thornton<sup>8</sup>, Steven S. Brown<sup>9,10</sup>,  
7 Astrid Kiendler-Scharr<sup>1</sup>, Andreas Wahner<sup>1</sup>, Mattias Hallquist<sup>3</sup>, Thomas F. Mentel<sup>1\*</sup>

8 <sup>1</sup>Institute of Energy and Climate Research, Troposphere (IEK-8), Forschungszentrum Jülich GmbH, 52428  
9 Jülich, Germany

10 <sup>2</sup>College of Environmental Sciences and Engineering, State Key Joint Laboratory of Environmental Simulation  
11 and Pollution Control, Peking University, 100871, Beijing, China

12 <sup>3</sup>Department of Chemistry and Molecular Biology, University of Gothenburg, 41296, Gothenburg, Sweden

13 <sup>4</sup>Department of Atmospheric and Oceanic Sciences & Institute of Atmospheric Sciences, Fudan University,  
14 200438, Shanghai, China

15 <sup>5</sup>Atmospheric Chemistry Department, Max Planck Institut für Chemie, 55128 Mainz, Germany

16 <sup>6</sup>Institut de Combustion, Aérothermique, Réactivité et Environnement (ICARE), UPR CNRS, 45071 Orléans,  
17 France

18 <sup>7</sup>Department of Chemistry, Reed College, Portland, OR 97202, USA

19 <sup>8</sup>Department of Atmospheric Sciences, University of Washington, Seattle, WA 98195, USA

20 <sup>9</sup>NOAA Chemical Sciences Laboratory, Boulder, CO 80305, USA

21 <sup>10</sup>Department of Chemistry, University of Colorado, Boulder, CO 80309, USA

22 <sup>a</sup>present address: SOLIDpower GmbH, 52525 Heinsberg, Germany

23 \*Correspondence to: Thomas F. Mentel (t.mentel@fz-juelich.de)

24

### 25 **Abstract**

26 Isoprene oxidation by nitrate radical (NO<sub>3</sub>) is a potentially important source of secondary organic aerosol (SOA).  
27 It is suggested that the second or later-generation products are the more substantial contributors to SOA.  
28 However, there are few studies investigating the multi-generation chemistry of isoprene-NO<sub>3</sub> reaction, and  
29 information about the volatility of different isoprene nitrates, which is essential to evaluate their potential to  
30 form SOA and determine their atmospheric fate, is rare. In this work, we studied the reaction between isoprene  
31 and NO<sub>3</sub> in the SAPHIR chamber (Jülich) under near atmospheric conditions. Various oxidation products were  
32 measured by a high-resolution time-of-flight chemical ionization mass spectrometer using Br<sup>-</sup> as the reagent ion.  
33 They are grouped into monomers (C<sub>4</sub>- and C<sub>5</sub>-products), and dimers (C<sub>10</sub>-products) with 1–3 nitrate groups  
34 according to their chemical composition. Most of the observed products match expected termination products  
35 observed in previous studies, but some compounds such as monomers and dimers with three nitrogen atoms  
36 were rarely reported in the literature as gas-phase products from isoprene oxidation by NO<sub>3</sub>. Possible formation  
37 mechanisms for these compounds are proposed. The multi-generation chemistry of isoprene and NO<sub>3</sub> is  
38 characterized by taking advantages of the time behavior of different products. In addition, the vapor pressures of  
39 diverse isoprene nitrates are calculated by different parametrization methods. An estimation of the vapor  
40 pressure is also derived from their condensation behavior. According to our results, isoprene monomers belong  
41 to intermediate volatility or semi-volatile organic compounds and thus have little effect on SOA formation. In  
42 contrast, the dimers are expected to have low or extremely low volatility, indicating that they are potentially



43 substantial contributors to SOA. However, the monomers constitute 80% of the total explained signals on  
44 average, while the dimers contribute less than 2%, suggesting that the contribution of isoprene NO<sub>3</sub> oxidation to  
45 SOA by condensation should be low under atmospheric conditions. We expect a SOA mass yield of about 5 %  
46 from the wall loss and dilution corrected mass concentrations, assuming that all of the isoprene dimers in the  
47 low- or extremely low-volatility organic compound (LVOC or ELVOC) range will condense completely.



## 48 1. Introduction

49 Atmospheric submicron aerosols have an adverse effect on air quality, human health and climate (Jimenez et al.,  
50 2009; Pöschl, 2005). Secondary organic aerosol (SOA), which is formed from oxidation of volatile organic  
51 compounds (VOC) followed by gas-to-particle partitioning, comprise a large fraction (20-90%) of the  
52 submicron aerosol mass (Jimenez et al., 2009; Zhang et al., 2007). It is confirmed that a significant proportion of  
53 SOA arises from biogenic VOC (BVOC) oxidation (Hallquist et al., 2009; Spracklen et al., 2011).

54 Isoprene is globally the most abundant non-methane volatile organic compound originating from  
55 vegetation, with emissions estimated to be 440-660 Tg yr<sup>-1</sup> (Guenther et al., 2012). Due to its high abundance, as  
56 well as its high reactivity with atmospheric oxidants, isoprene plays a significant role in tropospheric chemistry,  
57 and its chemistry affects the global aerosol burden and distribution (Carlton et al., 2009; Fry et al., 2018; Ng et  
58 al., 2008, 2017; Surratt et al., 2010), although its SOA yield is much lower than those of monoterpenes and  
59 sesquiterpenes (Friedman and Farmer, 2018; Kim et al., 2015; Marais et al., 2016; , McFiggans, et al. 2019;  
60 Mutzel et al., 2016; Ng et al., 2007, 2008; Surratt et al., 2010; Thornton et al., 2020). Recent model simulations  
61 suggested the isoprene-derived SOA production is 56.7 Tg C yr<sup>-1</sup>, contributing up to 41% of global SOA  
62 (Stadtler et al., 2018). Observations in southeastern United States suggested that isoprene-derived SOA makes  
63 up 17- 48% of total organic aerosol (Hu et al., 2015; Kim et al., 2015; Marais et al., 2016). As a consequence, it  
64 is essential to fully characterize the potential of isoprene to form condensable products and its contribution to  
65 SOA formation (Carlton et al., 2009).

66 Generally, isoprene is primarily oxidized by the hydroxyl radical (OH) and somewhat by ozone (O<sub>3</sub>) in the  
67 daytime. At night when the concentration of OH is negligible, the nitrate radical (NO<sub>3</sub>) and O<sub>3</sub> become the  
68 predominant oxidants of isoprene. Reaction of isoprene with NO<sub>3</sub> is competitive to that with O<sub>3</sub> because of its  
69 much larger rate constant ( $k_{NO_3} = 6.5 \times 10^{-13} \text{ cm}^3 \text{ molecules}^{-1} \text{ s}^{-1}$  and  $k_{O_3} = 1.28 \times 10^{-17} \text{ cm}^3 \text{ molecules}^{-1} \text{ s}^{-1}$  at 298 K,  
70 respectively, IUPAC), even if the mixing ratio of NO<sub>3</sub> is 10,000 time lower than that of O<sub>3</sub>. Although reaction  
71 with NO<sub>3</sub> only represents ~ 5-6% of isoprene loss, it accounts for a large proportion of isoprene nitrates (~ 40-  
72 50%) (Wennberg et al., 2018). Therefore, reaction of isoprene with NO<sub>3</sub> is a potential source of SOA. In  
73 addition, it is found from both laboratory and chamber experiments that the SOA yield of isoprene from NO<sub>3</sub>  
74 oxidation is higher than that from OH or O<sub>3</sub> oxidation, which is typically less than 5% (Carlton et al., 2009;  
75 Dommen et al., 2009; Kleindienst et al., 2007; Kroll et al., 2006). For example, Ng et al. (2008) concluded the  
76 isoprene SOA yield from NO<sub>3</sub> was in the range of 4.3% to 23.8%, depending on RO<sub>2</sub> fate (higher SOA yield  
77 when the experiments were dominated by RO<sub>2</sub>+RO<sub>2</sub> rather than RO<sub>2</sub>+NO<sub>3</sub> reaction). Rollins et al. (2009) also  
78 observed a high SOA yield from isoprene (14%) when both of its double bonds were oxidized by NO<sub>3</sub>. In an  
79 aircraft study in the southeastern United States, Fry et al. (2018) derived an isoprene-NO<sub>3</sub> SOA yield as large as  
80 27% on average under high NO<sub>x</sub> conditions, although their mass yield estimation was indirect, and based on a  
81 molar yield determination of  $9 \pm 5\%$ . In light of the relatively high SOA yield from NO<sub>3</sub> oxidation, even though  
82 only a minor fraction of isoprene is oxidized by NO<sub>3</sub>, the SOA formed at nighttime would still probably be  
83 comparable to that produced at daytime (Brown et al., 2009; Fry et al., 2018).

84 However, isoprene-NO<sub>3</sub> chemistry has received less attention than the extensively studied OH- or O<sub>3</sub>-  
85 initiated oxidation (Barber et al., 2018; Novelli et al., 2020; Peeters et al., 2014; Wang et al., 2018; Wennberg et  
86 al., 2018; Whalley et al., 2012). It has been recognized that later-generation oxidation of isoprene by NO<sub>3</sub> makes  
87 more significant contribution to SOA formation (Carlton et al., 2009; Fry et al., 2018; Rollins et al., 2009).



88 Nevertheless, although the importance of multi-generation  $\text{NO}_3$  oxidation of isoprene to SOA formation has  
89 been recognized, few studies extended the investigation beyond the first-generation oxidation, and details of  
90 isoprene- $\text{NO}_3$  multi-generation chemistry are still lacking.

91 Organic compounds, especially highly oxygenated organic molecules (HOM) that have low or extremely  
92 low volatility, contribute significantly to SOA formation by condensation, or even form new particles (Bianchi  
93 et al., 2019; Ehn et al., 2014; Kirkby et al., 2016, Tröstl et al., 2016). Previous studies have confirmed that low-  
94 volatility products from isoprene- $\text{NO}_3$  reaction are the major precursors to SOA (Ng et al., 2008; Rollins et al.,  
95 2009; Schwantes et al., 2019). Here the low-volatility compounds refer to gas phase products that allow  
96 fractions to exist in particle-phase, and may include the groups of organic compounds with intermediate  
97 volatility (IVOC,  $300 < C^* < 3 \times 10^6 \mu\text{g m}^{-3}$ ), semi-volatility (SVOC,  $0.3 < C^* < 300 \mu\text{g m}^{-3}$ ), low volatility (LVOC,  
98  $3 \times 10^{-5} < C^* < 0.3 \mu\text{g m}^{-3}$ ) and extremely low volatility (ELVOC,  $C^* < 3 \times 10^{-5} \mu\text{g m}^{-3}$ ) as proposed by Donahue et al.  
99 (2012). In general, SVOC, LVOC and ELVOC can contribute to the SOA formation (Jimenez et al., 2009). In  
100 order to evaluate the potential of oxygenated products to form SOA, information about their vapor pressures is  
101 essential. However, due to the high degree of functionalization, low or extremely low volatility, as well as  
102 uncertainties in quantification and molecular structures, it is challenging to determine the exact vapor pressure  
103 of highly oxidized products. Detailed information on the volatilities of different generation products is lacking,  
104 which impedes the assessment of their contribution to SOA formation.

105 In this work, we present the results of chamber experiments on isoprene oxidation by  $\text{NO}_3$  under near  
106 atmospheric conditions, where  $\text{NO}_3$  was produced in situ by  $\text{O}_3$  reaction with  $\text{NO}_2$ . Subsequent characteristics of  
107 multi-generation chemistry of isoprene with  $\text{NO}_3$  are investigated. By examining the time evolution of various  
108 gas-phase products, we propose possible reaction mechanisms that help to get the possible functionalization of  
109 the products. Saturation vapor pressures of the major gas-phase products observed by HR-ToF-CIMS are  
110 predicted by using different parameterization methods that are widely-used or state-of-the-art in literature. In  
111 addition, we estimate the vapor pressure derived from equilibrium partitioning coefficient according to the  
112 condensation behavior of different products in experiments with and without seed aerosols. Based on these  
113 results, the volatility of the major oxidation products stemming from isoprene- $\text{NO}_3$  reaction and their potential  
114 to form SOA are evaluated.

## 115 2. Experimental and methods

### 116 2.1 Atmospheric simulation chamber SAPHIR

117 All the data presented here were measured in the atmospheric simulation chamber SAPHIR (Simulation of  
118 Atmospheric PHotochemical In a large Reaction Chamber) at Forschungszentrum Jülich, Germany, which is  
119 designed to investigate the oxidation processes of both biogenic and anthropogenic trace gases and formation of  
120 secondary particles and pollutants under near atmospheric conditions. The SAPHIR chamber is a double-walled  
121 Teflon (FEP) cylinder with a volume of  $270 \text{ m}^3$  (5 meters in diameter and 18 meters in length). The large  
122 volume-to-surface ratio (1 m) allows experiments to be conducted under natural conditions and reduces  
123 interference from the chamber walls. The chamber is equipped with a shutter system which can be opened to  
124 admit sunlight for photochemical experiments or closed to mimic nighttime conditions. There are two fans  
125 inside the chamber to ensure good mixing of trace gases (within 2 minutes). The chamber is filled with synthetic



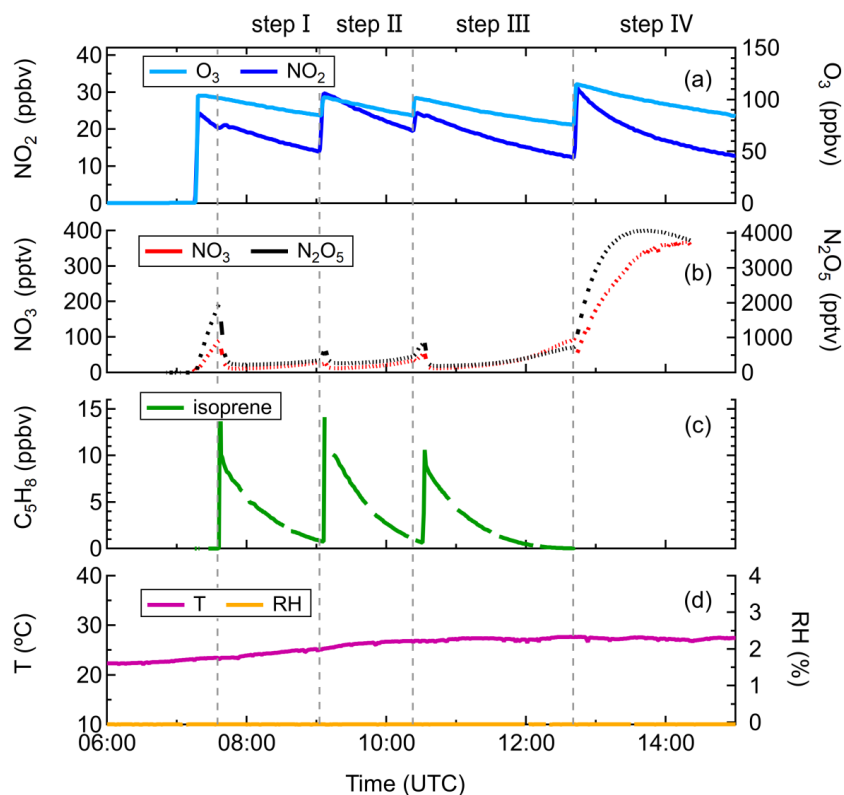
126 air made from mixing of ultrapure nitrogen and oxygen (Linde, purity  $\geq 99.99990\%$ ) and is slightly over-  
127 pressured ( $\sim 35$  Pa) to prevent intrusion of outside air into the chamber. Due to small leakage ( $\sim 7$  m<sup>3</sup> h<sup>-1</sup>) and  
128 gas consumption by instrument sampling, a replenishment flow is provided by a flow control, which leads to a  
129 dilution rate of 4%–7% per hour. A more detailed description of the chamber set-up and its characterization can  
130 be found elsewhere (Rohrer et al., 2005).

## 131 2.2 Experiment description

132 A series of experiments investigating the oxidation of isoprene by NO<sub>3</sub> were conducted in the SAPHIR chamber  
133 in August 2018 (ISOPNO<sub>3</sub> campaign) under different chemical conditions. In this work, we primarily focus on  
134 an experiment conducted on 08 August 2018 that examined the fast oxidation of isoprene by NO<sub>3</sub> (up to  $\sim 130$   
135 pptv) without seed aerosols. The experiment was performed under dry (RH < 5%) and dark condition, and  
136 employed injections of O<sub>3</sub> and NO<sub>2</sub> as source of NO<sub>3</sub>, where O<sub>3</sub> was generated by a silent discharge ozoniser  
137 (O3onia), and high-purity NO<sub>2</sub> was introduced from a gas bottle (Linde, purity >99%).

138 Before the experiment, the chamber was flushed overnight with a total amount of  $\sim 1800$  m<sup>3</sup> synthetic air to  
139 minimize any remaining contamination. At the beginning of the experiment, the chamber air was slightly  
140 humidified (RH < 0.1%) by flushing water vapor from boiling Milli-Q<sup>®</sup> water into the chamber. Thereafter, O<sub>3</sub>  
141 and NO<sub>2</sub> were added to the chamber in succession, and their concentrations in the chamber after injection were  
142 approximately 100 and 25 ppbv, respectively, as shown in Fig. 1. After that,  $\sim 10$  ppbv of isoprene was injected  
143 using a GC syringe, initiating the reaction with NO<sub>3</sub>. The period between the first and second injection is  
144 defined as “step I”, as so on for the other three periods. After almost complete consumption of isoprene, another  
145  $\sim 100$ , 30, and 10 ppbv of O<sub>3</sub>, NO<sub>2</sub>, and isoprene, respectively, were added. After another  $\sim 1.5$  hours, the  
146 chemistry was accelerated again by the third injection, and the concentrations of O<sub>3</sub>, NO<sub>2</sub>, and isoprene reached  
147  $\sim 100$ , 25, and 10 ppbv, respectively, after the injection. Two hours later, the fourth addition was made and the  
148 concentrations of O<sub>3</sub> and NO<sub>2</sub> increased to approximately 115 ppbv and 30 ppbv, respectively, aiming to  
149 promote further oxidation of early generation products. In total the system was kept running for about 7.5 h.  
150 According to the modeling results, approximately 90% of the isoprene reacted with NO<sub>3</sub>, indicating that reaction  
151 with O<sub>3</sub> was a minor sink of isoprene in our system.

152 A complementary experiment was conducted on 14 August 2018 under similar conditions but with seed  
153 aerosols. Approximately 60  $\mu\text{g m}^{-3}$  of ammonium sulfate aerosol was added at the beginning of the experiment.  
154 Thereafter, approximate 100 and 20 ppbv of O<sub>3</sub> and NO<sub>2</sub> were introduced to the chamber to produce NO<sub>3</sub>,  
155 followed by addition of  $\sim 10$  ppbv of isoprene in about 30 minutes later (see Fig. S1). Another 6 ppbv of NO<sub>2</sub>  
156 and 10 ppbv of isoprene were added about one hour later to accelerate the reaction. At the last injection, only O<sub>3</sub>  
157 ( $\sim 50$  ppbv) and NO<sub>2</sub> ( $\sim 7$  ppbv) were added, similar as for the experiment without seeds. The experiment lasted  
158 for about 8 h. The results were used to investigate the condensation behavior of various gas-phase products from  
159 isoprene oxidation, aiming to estimate equilibrium partitioning coefficients and vapor pressures.



160

161 **Figure 1: Measurements of (A) O<sub>3</sub> and NO<sub>2</sub>, (B) NO<sub>3</sub> and N<sub>2</sub>O<sub>5</sub>, (C) isoprene and (D) temperature and relative**  
162 **humidity in the chamber during the experiment on 08 August, 2018.**

### 163 2.3 Instrumentation

164 A high-resolution time-of-flight chemical ionization mass spectrometer (HR-ToF-CIMS, Aerodyne Research  
165 Inc., hereafter CIMS) was used to continuously measure the gas-phase products from isoprene oxidation by NO<sub>3</sub>.  
166 The ToF-MS was operated in 'V' mode with the mass resolution power between 3000–4000 Th/Th. In order to  
167 reduce the losses of HO<sub>2</sub> radicals and HOM on the tubing, a customized inlet (Albrecht et al., 2019) was directly  
168 connected to the chamber. The CIMS was operated in negative ion mode using Br<sup>-</sup> as the reagent ion, which is  
169 selective to polar species such as acids, hydroxy or nitrooxy carbonyls, as well as HO<sub>2</sub> radicals (Albrecht et al.,  
170 2019; Ng et al., 2008; Rissanen et al., 2019; Riva et al., 2019).

171 Bromide ions were generated by passing a mixture of 10 standard cubic centimeters per minute of 0.4%  
172 CF<sub>3</sub>Br in nitrogen and 2 standard liter per minute nitrogen through a 370 MBq <sup>210</sup>Po source (Type P-2021-5000,  
173 NDR Static Control LLC, USA), resulting in ~10<sup>5</sup> ion counts per second (Albrecht et al., 2019). In our system,  
174 most compounds were detected as adducts with Br<sup>-</sup>, but some strong acidic compounds like nitric acid were also  
175 detected as deprotonated ions. The isotope distribution of <sup>79</sup>Br and <sup>81</sup>Br is approximately 1:1, therefore two  
176 signals appear at  $m/z = MW+79$  and  $m/z = MW+81$  with MW being the molecular mass of the molecule that is  
177 detected as cluster with Br<sup>-</sup>. In this work, we will use Thomson (Th) as the unit for mass-to-charge ( $m/z$ ), and the



178  $m/z$  of molecules discussed in following include the mass contribution from  $\text{Br}^-$  ( $m/z$  79) if there is no other  
179 annotation.

180 In order to have an indicator of the CIMS performance, perfluoropentanoic acid (PFPA) was used as an  
181 internal standard. The CIMS was optimized to gain a maximum signal of  $[\text{HO}_2^*\text{Br}]^-$  isotopes, which are weakly  
182 bounded clusters. This was achieved by adjusting step by step the electrostatic field in the transfer stage to  
183 minimize fragmentation. During the campaign, the settings of CIMS were kept unchanged to keep a similar  
184 performance. However, the signal of reagent ion  $\text{Br}^-$  decreased by about 65% (from ~ 100, 000 to 34, 000 counts  
185  $\text{s}^{-1}$ ) over the campaign duration of four weeks. In order to minimize the effect of drift in performance, we used  
186 the normalized (by the sum of the total ion counts) signals for analysis. The sensitivity for total carbon was  
187 calculated by determining the slope of wall-loss corrected total carbon signals detected by CIMS (only the  
188 identified peaks were considered) versus isoprene consumed. As illustrated in Fig. S2a, the CIMS sensitivities  
189 were roughly identical in two experiments ( $0.026 \pm 0.002$  norm. count  $\text{s}^{-1}$  ppbv $^{-1}$  on 08 August, and  $0.022 \pm$   
190  $0.001$  norm. count  $\text{s}^{-1}$  ppbv $^{-1}$  on 14 August), indicating that different experimental conditions over two days had  
191 an insignificant impact on CIMS sensitivity for total carbon and thus the data from these days are comparable.  
192 In addition, an inter-comparison of measurements by  $\text{Br}^-$  CIMS and  $\text{I}^-$  CIMS were made. As shown in Fig. S2b,  
193 the measurements of  $\text{C}_5\text{H}_6\text{N}_2\text{O}_8$  from the two instruments are well linearly correlated with each other at the early  
194 oxidation stages. However, the correlation coefficient somewhat changes between the two experiments, which is  
195 possibly related to the interference from isomers and the differences in sensitivity between the two instruments.  
196 In general, the performance of  $\text{Br}^-$  CIMS was stable and the data taken by it are reliable.

197 The mass spectra data were processed using the software “Tofware” embedded in Igor as provided by  
198 Aerodyne Research Inc. (<https://www.tofwerk.com/software/tofware/?cn-reloaded=1>). Peaks detected in the  
199 mass spectra could be isolated and identified according to their exact mass, and molecular formulas and the  
200 corresponding intensities were obtained by high-resolution peak fitting. Due to a lack of authentic standards for  
201 the products, it is difficult to quantitatively determine their individual absolute concentrations, but we have  
202 calculated the bulk sensitivity for organonitrates by determining the slope of total organic nitrate signals  
203 detected by  $\text{Br}^-$  CIMS versus the alkyl nitrate concentrations measured by a thermal dissociation cavity ring-  
204 down spectrometer, as shown in Fig. S2c. The estimated bulk sensitivities for organonitrates are  $0.016 \pm 0.001$   
205 and  $0.022 \pm 0.001$  norm. count  $\text{s}^{-1}$  ppbv $^{-1}$  on 08 August and 14 August, respectively, comparable to the sensitivity  
206 for total carbon, but smaller than the sensitivity for salicylic acid determined by an independent calibration ( $163$   
207 norm. count  $\mu\text{g}^{-1}$  on average as shown in Fig. S2d, equal to  $0.07$  norm. count  $\text{s}^{-1}$  ppbv $^{-1}$ ). The bulk sensitivity for  
208 organonitrates enables estimation of the absolute concentrations of products assuming that they have identical  
209 sensitivity. In this study we use the normalized signals instead of absolute concentrations for analysis. This is  
210 sufficient here because our analysis focuses on the time evolution of signals and the relative changes of  
211 intensities, so the absolute concentrations are not necessarily needed. The sensitivity derived above is only used  
212 to convert the signals of dimers to concentrations in order to estimate the SOA yield.

213 Isoprene was measured by a Vocus proton transfer reaction time-of-flight mass spectrometer (Aerodyne  
214 Research Inc., hereafter Vocus), which has a higher mass resolving power (nominal 10000 Th/Th) and less inlet  
215 wall losses and sampling delays compared to traditional PTR-MS (Krechmer et al., 2018). The mixing ratio of  
216  $\text{O}_3$  was monitored by an UV absorption instrument, and that of  $\text{NO}_2$  was monitored by a chemiluminescence  
217 instrument and a custom-built cavity ring-down spectrometer (CRDS). The concentrations of  $\text{NO}_3$  and  $\text{N}_2\text{O}_5$



218 were detected by two custom-built CRDS instruments (Dubé et al., 2006; Sobanski et al., 2016). In addition,  
219 temperature and pressure inside the chamber were monitored by an ultra-sonic anemometer and a pressure  
220 sensor, respectively. The relative humidity was primarily detected as water mixing ratio by a Picarro CRDS  
221 instrument (Crosson, 2008).

222 The particle number concentrations and their size distributions were measured by a condensation particle  
223 counter (TSI 3783, hereafter CPC) and a scan mobility particle sizer (TSI 3081 electrostatic classifier combined  
224 with TSI 3025 CPC, hereafter SMPS). The aerosol chemical composition was identified by a high-resolution  
225 time of flight aerosol mass spectrometer (HR-ToF-AMS, Aerodyne Research Inc., hereafter AMS). The  
226 ionization efficiency of AMS was determined by using the monodisperse aerosol generated from  $\text{NH}_4\text{NO}_3$  and  
227  $(\text{NH}_4)_2\text{SO}_4$  solutions. The collection efficiency (CE) could be estimated based on the particle mass concentration  
228 yielded from AMS and that derived from SMPS. In this study, the average CE value of 0.5 is used for correction.

#### 229 **2.4 Methods to estimate saturation vapor pressure**

230 The pure liquid saturation vapor pressure is a thermodynamic metric relevant for the partitioning equilibrium of  
231 organic molecules, which determines their propensity to form SOA (Compernelle et al., 2011; O'Meara et al.,  
232 2014; Pankow and Asher, 2008). Due to their complex functionalities and low or extremely low volatility, it is  
233 challenging to determine the vapor pressures of highly oxidized molecules. As a result, theoretical and  
234 semiempirical methods are usually used for vapor pressure estimation. Commonly used semiempirical methods  
235 include composition-activity (CA), group-contribution (GC), and structure-activity (SA) methods. The CA  
236 methods are the easiest to use, as they only require information on molecular composition for estimation. They  
237 are widely applied in context of the two-dimensional volatility basis set (2D-VBS) (Donahue et al., 2011). For  
238 GC methods, the exact functional groups are required to calculate the saturation vapor pressure. The SIMPOL.1  
239 (Pankow and Asher, 2008), the parameterization as described by Nannoolal et al. (2008), and EVAPORATION  
240 (Compernelle et al., 2011) are three widely used GC methods. Structure-activity methods can provide more  
241 accurate estimates with sophisticated treatments of intramolecular interactions like intramolecular hydrogen-  
242 bonding (Bilde et al., 2015). However, detailed molecular properties such as boiling point and evaporation  
243 enthalpy are required for estimation, which are generally obtained by complex and time-consuming quantum  
244 chemical calculations. Therefore, SA methods are not applied for vapor pressure estimation in this study.

245 Saturation concentration ( $C^*$ , mass based) is related to saturation vapor pressure and can be calculated  
246 following Eq. (1) (Donahue et al., 2006). The  $\log_{10}(C^*)$  is a metric used in the 2D-VBS method to evaluate the  
247 volatility of organic molecules.

$$248 \quad C_i^* = \frac{M_i 10^6 \zeta_i p_i^\circ}{RT} \quad (1)$$

249 where  $R$  ( $8.206 \times 10^{-5} \text{ m}^3 \text{ atm K}^{-1} \text{ mol}^{-1}$ ) is the gas constant,  $T$  (K) is the temperature,  $M_i$  ( $\text{g mol}^{-1}$ ) is the molecular  
250 weight of compound  $i$ ,  $\zeta_i$  is the activity coefficient of compound  $i$  and here is assumed to be 1 (Donahue et al.,  
251 2006),  $p_i^\circ$  (atm) is the pure liquid saturation vapor pressure at temperature  $T$  (298 K).

252 In this study, different CA methods are applied to calculate the saturation vapor pressures of various  
253 oxidation products from isoprene reaction with  $\text{NO}_3$ . These include parameterizations that were constrained by  
254 chamber measurements as proposed by Donahue et al. (2011), Mohr et al. (2019), and Peräkylä et al. (2019).  
255 Further we test the GC methods proposed by Nannoolal et al. (2008), Pankow and Asher (2008, SIMPOL.1),





256 and Compernelle et al. (2011, EVAPORATION). All the methods used in this study are summarized in Table 1.  
257 The calculations of EVAPORATION and the Nannool method were done via the online molecular and  
258 multiphase property prediction facility UManSysProp  
259 ([http://umansysprop.seaes.manchester.ac.uk/tool/vapour\\_pressure](http://umansysprop.seaes.manchester.ac.uk/tool/vapour_pressure)). For the latter the boiling point  
260 parameterization method needs to be predefined, and that from Nannoolal et al. (2004) was adopted as  
261 recommended by O'Meara et al. (2014). The information about molecular structures needed for the calculation  
262 is inferred from mechanistic information, which is described in detail in Sect. 2.5.

263 **Table 1: Summary of estimation methods of saturation vapor pressure used in this study**

Estimation method	Methodology	Input information			Reference
		molecular formula	functional groups	others	
Donahue et al.	CA <sup>a</sup>	√			Donahue et al., 2011
Mohr et al.	CA	√			Mohr et al., 2019
Peräkylä et al.	CA	√			Peräkylä et al., 2020
Nannoolal et al.	GC <sup>b</sup>	√	√	√ <sup>d</sup>	Nannoolal et al., 2008
SIMPOL.1	GC	√	√		Pankow and Asher, 2008
EVAPORATION	GC	√	√		Compernelle et al., 2011
This study	EXP <sup>c</sup>				

264 <sup>a</sup> abbreviation of composition-activity method; <sup>b</sup> abbreviation of group-contribution method; <sup>c</sup> abbreviation of  
265 experimental method; <sup>d</sup> boiling point parameterization method is also required to be defined.

266 In addition, we take advantage of the measurements in this study to calculate the gas-particle equilibrium  
267 partitioning coefficient (K) by comparing experiments with and without seed aerosols. The partitioning  
268 coefficient K can be converted to saturation concentration C\* by Eq. (2).

$$269 K_i = \frac{C_{i,p}}{C_{i,g} \times C_{OA}} = \frac{1}{C_i^*} \quad (2)$$

270 where  $C_{i,g}$  and  $C_{i,p}$  are the gas- and particle-phase concentrations ( $\mu\text{g m}^{-3}$ ) of species  $i$ , respectively, and  $C_{OA}$  is  
271 the organic aerosol concentration ( $\mu\text{g m}^{-3}$ ). In this study,  $C_{i,g}$  is signal of species  $i$  from CIMS in the experiment  
272 with seeds, and  $C_{i,p}$  is the difference of signals between experiment without and with seeds (under the same  
273 isoprene consumption condition). The  $C_{OA}$  in the experiment with seeds is in a range of 1-4  $\mu\text{g m}^{-3}$ .

## 274 2.5 Pathways to the multifunctional oxidation products

### 275 2.5.1 Basic peroxy and alkoxy radical chemistry

276 As mentioned before, information about molecular structures (at least functional groups) is required to calculate  
277 vapor pressures by using GC methods. Although the high-resolution ToF-CIMS allows for determining  
278 chemical composition of the detected ions, it is unable to provide information about molecular structures, so that  
279 the constitutional or configurational isomers with the same mass cannot be distinguished without additional



280 information. Fortunately, knowledge of detailed chemical formation mechanisms can help inferring the  
281 molecular structure information. However, the development of a comprehensive, multi-generational kinetic  
282 mechanism for NO<sub>3</sub>-initiated oxidation of isoprene is outside the scope of the current paper. Instead, in order to  
283 link the observed mass peaks to representative molecular structures, we developed a framework tracing the  
284 chemical oxidation mechanisms by taking well-known oxidation steps to predict the most likely isomeric forms  
285 of the functionalized products formed in the isoprene oxidation. For this purpose, we rely on the extensive  
286 literature on isoprene, alkylperoxy radical, and alkoxy radical chemistry (Atkinson, 2007; Atkinson and Arey,  
287 2003; Bianchi et al., 2019; Crouse et al., 2013; Ehn et al., 2014; Jenkin et al., 2015; Kwan et al., 2012; Mentel  
288 et al., 2015; Ng et al., 2008; Orlando et al., 2003; Orlando and Tyndall, 2012; Rollins et al., 2009; Schwantes et  
289 al., 2015; Vereecken and Francsico, 2012; Vereecken and Peeters, 2010; Wennberg et al., 2018; Ziemman and  
290 Atkinson, 2012). This framework is depicted in the supporting information and will be discussed in more detail  
291 in Sect. 2.5.2 and Sect. 2.5.3. They are based on the following main reactivity trends.

292 Generally, RO<sub>2</sub> radicals can react with other RO<sub>2</sub> and HO<sub>2</sub> radicals. There are three major channels for the  
293 reaction between two RO<sub>2</sub> radicals, leading to alkoxy radicals (RO) (Reaction R1a), as well as termination  
294 products like alcohols, aldehydes or ketones (Reaction R1b) and accretion products (Reaction R1c). These  
295 reactions should take place with the first-generation peroxy radicals, as well as with the higher generation RO<sub>2</sub>  
296 radicals formed in the later oxidation steps. Hydroperoxides can be formed from the reaction of RO<sub>2</sub> with HO<sub>2</sub>  
297 radicals (Reaction R2a). This reaction can also yield alkoxy radicals (Reaction R2b).



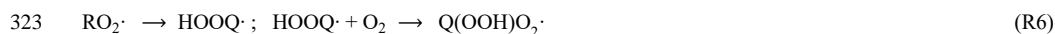
303 In the presence of NO<sub>x</sub>, RO<sub>2</sub> radicals can also react with NO and NO<sub>2</sub>, leading to the formation of alkoxy  
304 radicals (R3a), organic nitrates (R3b), and peroxy nitrates (R4) (including peroxyacyl nitrates, PANs, if R =  
305 R'C(O)-). The channel that results in RO radicals is the major pathway for the reaction of RO<sub>2</sub> radicals with NO  
306 (Ziemann and Atkinson, 2012). However, reactions of RO<sub>2</sub> radicals with NO (Reaction R3a and R3b) can be  
307 neglected in this study due to the high O<sub>3</sub> concentration, which results in rapid conversion of NO to NO<sub>2</sub>. The  
308 peroxy nitrates formed from the reaction of RO<sub>2</sub> with NO<sub>2</sub> will undergo rapid thermal decomposition under our  
309 experimental conditions, with exception of PANs. The reaction of RO<sub>2</sub> with NO<sub>3</sub> radicals mainly forms NO<sub>2</sub> and  
310 alkoxy radicals (Reaction R5), which will continue the radical chains (Reaction R7).



315 In addition to bimolecular reactions, intramolecular rearrangement (H-migration) is a competitive reaction  
316 pathway for RO<sub>2</sub> radicals. RO<sub>2</sub> radicals can undergo H-migration to form a hydroperoxy functionality (-OOH)  
317 and a radical site that can subsequently recombine with an O<sub>2</sub> molecule, leading to the formation of a new, more  
318 oxidized substituted RO<sub>2</sub> (Reaction R6). This process is the so-called “autoxidation” path and has been



319 confirmed as a significantly important way for SOA formation (Crouse et al., 2013; Ehn et al., 2014; Mentel et  
320 al., 2015; Praske et al., 2018; Rissanen et al., 2014). The rates of RO<sub>2</sub> H-migration are strongly dependent on the  
321 structure of RO<sub>2</sub> radicals, and the most likely routes can be derived based on the structure-activity relationship  
322 proposed by Vereecken and Nozière (2020).



324 The RO radicals formed in in the reaction of RO<sub>2</sub> + RO<sub>2</sub> typically have three accessible pathways,  
325 including isomerization by H-migration (Reaction R7a), fragmentation (Reaction R7b) and less important here,  
326 reaction with O<sub>2</sub> (Reaction R7c). Like H-migration in RO<sub>2</sub>, rearrangement by H-shift in RO radicals leads to the  
327 formation of more oxidized RO<sub>2</sub> radicals. Fragmentation leads to smaller carbon chains, and this becomes more  
328 important for alkoxy radicals with a higher number of (oxygen-bearing) substituents (Vereecken and Peeters,  
329 2009, 2010).



333 In addition to the above general reaction pathways, we include a number of other reactions in the  
334 framework, such as fragmentation of peroxy radicals, epoxidation of β-OOH alkyl radicals, and unimolecular  
335 termination of nitrooxy or hydroperoxyl peroxy radicals. Details can be found in the supporting information.

### 336 2.5.2 Formation of first-generation products

337 Here “first-generation products” refers to the closed-shell compounds from the first attack of NO<sub>3</sub> at the  
338 isoprene double bonds, while “second-generation products” follow an addition of NO<sub>3</sub> to the remaining double  
339 bond (or any other oxidation reaction) of a first-generation product. Addition of a NO<sub>3</sub> radical to one of isoprene  
340 double bonds and subsequent addition of O<sub>2</sub> to the resulting (delocalized) radical sites leads to the formation of  
341 nitrooxy alkylperoxy radicals (INO<sub>2</sub>, C<sub>5</sub>H<sub>8</sub>NO<sub>3</sub>). Since isoprene contains two double bonds, NO<sub>3</sub> can attack any  
342 of the four positions on the conjugated carbon bonds, resulting in eight possible INO<sub>2</sub> isomers (including six  
343 constitutional and two conformational isomers), as shown in Scheme S1. However, both theoretical and  
344 experimental studies suggest that the addition occurs preferably at the primary and terminal carbons, wherein C1  
345 addition seems to be preferred over C4 addition (Schwantes et al., 2015; Suh et al., 2001; Wennberg et al., 2018).  
346 As the GC methods have limited or no ability to distinguish between positional isomers (Kurten et al., 2016), we  
347 take exemplarily the products following the C1 addition for the vapor pressure analysis in this study.

348 The initial peroxy radicals (C<sub>5</sub>H<sub>8</sub>NO<sub>3</sub>) can undergo rearrangement by H shift from C–H bonds with  
349 subsequent O<sub>2</sub> addition, yielding new –OOH functionalized peroxy radicals (Reaction R6). Repeating this  
350 process can lead to the formation of a series of peroxy radicals and termination products with stepwise  
351 increasing number of oxygen atoms by 2, as shown in the conceptual scheme Scheme S2. This is the RO<sub>2</sub>  
352 autoxidation channel and the molecular formula of peroxy radicals formed via consecutive O<sub>2</sub> additions can be  
353 represented as C<sub>5</sub>H<sub>8</sub>NO<sub>(3+2n)</sub> (n ≥ 1, number of autoxidation steps). The autoxidation chain can be terminated  
354 when the H-shift occurs at a carbon with an –OOH or –ONO<sub>2</sub> group attached, leading to carbonyl formation  
355 with OH or NO<sub>2</sub> loss (Anglada et al., 2016; Bianchi et al., 2019; Vereecken, 2008; Vereecken et al., 2004). The



356 closed-shell products formed in these termination steps have the general molecular formula  $C_5H_7NO_{(5+2n-1)}$  (OH  
357 loss channel) or  $C_5H_8O_{(3+2n-2)}$  ( $NO_2$  loss channel).

358 The  $C_5H_8NO_{(3+2n)}$  peroxy radicals can also react with  $HO_2$  radicals to form  $-OOH$  functionalized  
359 termination products with the general molecular formula  $C_5H_9NO_{(3+2n)}$  (Reaction R2a), or yielding the alkoxy  
360 radicals  $C_5H_8NO_{(3+2n-1)}$  (Reaction R2b). In addition, the  $C_5H_8NO_{(3+2n)}$  peroxy radicals can react with other  $RO_2$   
361 radicals (Reaction R1a-R1c). The reaction R1a leads to the formation of alkoxy radicals ( $C_5H_8NO_{(3+2n-1)}$ ) while  
362 R1b forms closed-shell products either with a carbonyl group ( $C_5H_7NO_{(3+2n-1)}$ ) or a hydroxyl group  
363 ( $C_5H_9NO_{(5+2n-1)}$ ). Alternatively, dimers can be formed following Reaction R1c, which have then two  $-ONO_2$   
364 groups and at least 8 oxygen atoms depending on the formula of  $RO_2$  radicals involved, as shown in Table S1.

365 The alkoxy radicals from reactions R1a and R2b can undergo unimolecular rearrangement by H shift with  
366 subsequent  $O_2$  addition, similar to the  $RO_2$  radicals, forming new  $RO_2$  radicals with a  $-OH$  group (Reaction  
367 R7a). As mentioned above, when the H-shift occurs at a carbon with an  $-OOH$  or  $-ONO_2$  group attached, the  
368 resulting intermediates tend to lose an OH group or  $NO_2$  (Bianchi et al., 2019), yielding the closed-shell  
369 carbonyl products with general formulas  $C_5H_7NO_{(5+2n-2)}$  or  $C_5H_8O_{(3+2n-3)}$  respectively, as shown in the conceptual  
370 scheme Scheme S3. The newly-formed  $RO_2$  radicals from alkoxy H-shift channel can follow the peroxy  
371 pathways (Reaction R1-R6) like other  $RO_2$  radicals, leading to a diversity of compounds like hydroperoxides  
372 (Reaction R2a,  $C_5H_9NO_{(3+2n+1)}$ ), alcohols (Reaction R1b,  $C_5H_9NO_{(3+2n)}$ ), aldehydes (Reaction R1b,  $C_5H_7NO_{(3+2n)}$ )  
373 as well as accretion products (Reaction R1c,  $C_{10}H_{16}N_2O_x$ ), as depicted in Scheme S3. Alternatively, they can  
374 also yield alkoxy radicals again following reactions R1a and R2b and continue so on. Furthermore, the alkoxy  
375 radicals can break apart into two fragments according to Reaction R7b.

376 In general, the alkoxy reaction pathways diversify the parity of the oxygen number of the products from the  
377 reaction of isoprene with  $NO_3$ , and the compounds formed via these reactions generally have one less or one  
378 more oxygen atom compared to those formed from straight peroxy reaction pathways. With help of the  
379 mechanistic framework described above, we can infer the functionality of first-generation products. This is  
380 exemplified in Scheme S5 and S6 for the major first-generation  $C_5$  products. In addition, the reaction pathways  
381 and their corresponding structures of the first-generation  $C_{10}$  dimers ( $C_{10}H_{16}N_2O_x$ ) are summarized in Scheme  
382 S13.

### 383 2.5.3 Formation of second-generation products

384 Nitrate radicals can oxidize the first-generation products once again at the double bond remaining ( $k_{NO_3}(298K) \sim$   
385  $3-11 \times 10^{14} \text{ cm}^3 \text{ molecule}^{-1} \text{ s}^{-1}$ , Wennberg et al., 2018). This leads eventually to “second-generation” products that  
386 contain at least two nitrogen atoms. Addition of  $NO_3$  radical to the remaining double bond of the first-generation  
387 products results in the formation of dinitrooxy peroxy radicals. We assume that dinitrooxy peroxy radicals can  
388 undergo unimolecular and bimolecular reactions (Reaction R1–R6) in analogy to nitrooxy peroxy radicals,  
389 which lead to secondary products containing two or more nitrogen atoms, as summarized in the conceptual  
390 scheme Scheme S4.

391 The reaction of first-generation nitrooxy peroxy radicals with  $NO_2$  can also yield 2N-compounds (Reaction  
392 R4), however these 2N-compounds ought to be under first-generation products by definition. Such species are  
393 not discussed in detail here but will be covered to catch the diversity of the functionalities for the vapor pressure  
394 estimation. With the help of this secondary reaction framework, we can propose functional groups for the major



395 second-generation products. Scheme S8 – S10 depict the detailed (possible) reaction pathways that lead to the  
396 formation of detected C<sub>5</sub> dinitrates, as well as their possible structures. Furthermore, the proposed formation  
397 mechanism and their structures for C<sub>5</sub> trinitrates are shown in Scheme S12, while those for the second-  
398 generation C<sub>10</sub> dimers (C<sub>10</sub>H<sub>17</sub>N<sub>3</sub>O<sub>x</sub> and C<sub>10</sub>H<sub>18</sub>N<sub>4</sub>O<sub>x</sub>) are depicted in Scheme S13.

#### 399 **2.5.4 Formation of fragmentation products**

400 In addition to the multigenerational C<sub>5</sub> and C<sub>10</sub> products, fragmentation products can be formed from the  
401 reaction of isoprene with NO<sub>3</sub>. As mentioned above, the alkoxy radicals can undergo C–C bond scission,  
402 producing a carbonyl compound and an alkyl fragment (Reaction R7b). As shown in Scheme S7, when the  
403 secondary nitrooxy alkoxy radicals from the further oxidation of C<sub>5</sub> carbonyl compounds (C<sub>5</sub>H<sub>8</sub>O<sub>2</sub> and C<sub>5</sub>H<sub>8</sub>O<sub>3</sub>  
404 here) undergo unimolecular decomposition, C<sub>4</sub> carbonyl products (C<sub>4</sub>H<sub>7</sub>NO<sub>5</sub> and C<sub>4</sub>H<sub>7</sub>NO<sub>6</sub>, respectively) are  
405 formed as well as formyl radicals. Since the bond fission can occur at different positions, the generation of more  
406 reactive C<sub>2</sub> and C<sub>3</sub> carbonyl compounds are possible. In addition, the C<sub>4</sub> carbonyl compounds are possibly  
407 generated through peroxy radical arrangement by 1,4 H-shift and subsequent acyl radical bond scission reactions  
408 (see Scheme S7). The C<sub>4</sub> dinitrates can be formed following similar chemistry, as depicted in Scheme S11.

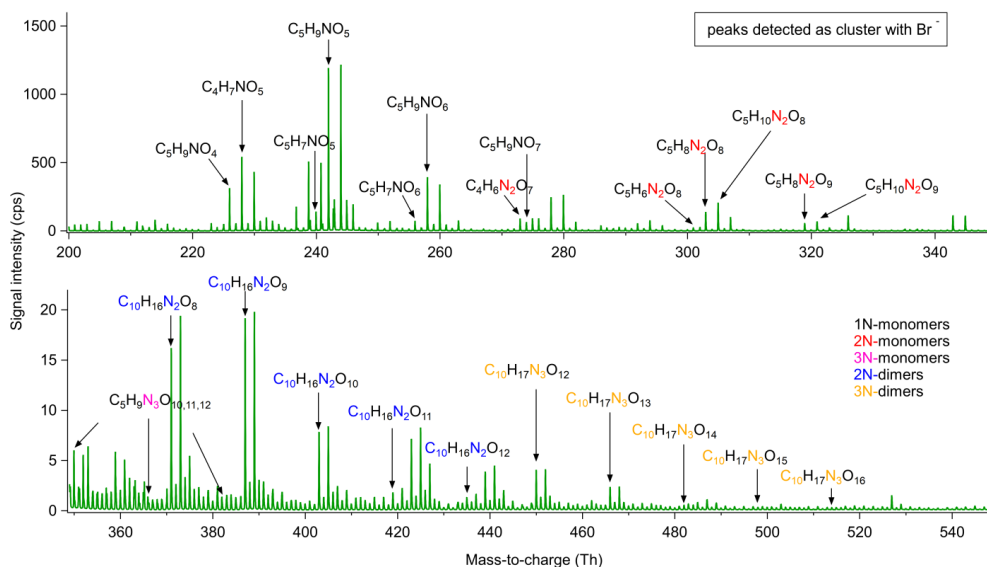
#### 409 **2.5.5 Candidate structures for vapor pressure estimation**

410 Among all gas-phase products detected by CIMS, we selected 32 major representative organonitrates formed  
411 from isoprene oxidation by NO<sub>3</sub> radicals. Their structures are rationalized by the corresponding molecular  
412 formulas and proposed formation mechanisms in the reaction framework. Table S2 summarizes all the  
413 exemplified structures used for vapor pressure estimation. The functional groups covered in the selected  
414 structures include nitrate, hydroxyl, ketone, aldehyde, carboxylic acid, peroxide, hydroperoxide, hydroperoxy  
415 acid, peroxyxynitrate, peroxyacyl nitrate and epoxide. The structural information allows calculation of the  
416 saturation vapor pressure by GC methods.

### 417 **3. Results and discussion**

#### 418 **3.1 Chemical composition of oxidation products**

419 Figure 2 illustrates the average mass spectra of the whole experiment measured by BrCIMS for isoprene-NO<sub>3</sub>  
420 reaction. Chemical sum formulas were attributed to most of the detected ions. The gas-phase products were  
421 separated into two major groups according to their chemical composition, including monomers comprising C<sub>5</sub>  
422 compounds and dimers containing C<sub>10</sub> compounds. There were also products from decomposition reactions with  
423 C<sub><5</sub>, which were merged into monomers. The monomers and dimers were further classified into five subgroups  
424 as follows. Monomers consisting of compounds with one nitrogen atom (hereafter 1N-monomers) and two or  
425 three N atoms (2N- or 3N-monomers) mainly accumulate in *m/z* 220–280 Th, *m/z* 300–340 Th and 350–390 Th,  
426 respectively, while dimers containing compounds with two N atoms (2N-dimers) and three N atoms (3N-dimers)  
427 appear in *m/z* 370–440 Th and 450–520 Th, respectively. As shown in Fig. 2, the signal intensities decrease  
428 from 1N-monomers, 2N-monomers, 2N-dimers to 3N-monomers and 3N-dimers. Many of the compounds  
429 detected in this work were also observed in previous isoprene-NO<sub>3</sub> systems (Kwan et al., 2012; Ng et al., 2008;  
430 Schwantes et al., 2015). In this work, only closed-shell products are considered for analysis.



431

432 **Figure 2: Averaged mass spectra for isoprene-NO<sub>3</sub> experiment on 8 August, 2018. Molecular formulas were**  
433 **determined according to the accurate mass data provided by HR-ToF-CIMS.**

434 The 1N-monomer C<sub>5</sub>H<sub>9</sub>NO<sub>5</sub> at *m/z* 242 is the dominant product formed from the NO<sub>3</sub>-induced isoprene  
435 oxidation in our experiment, followed by the 1N-decomposition product C<sub>4</sub>H<sub>7</sub>NO<sub>5</sub> at *m/z* 228. In addition to  
436 C<sub>5</sub>H<sub>9</sub>NO<sub>5</sub>, several analogues with molecular formulas C<sub>5</sub>H<sub>7</sub>NO<sub>4-7</sub> and C<sub>5</sub>H<sub>9</sub>NO<sub>4</sub> are in relatively high abundance.  
437 C<sub>5</sub>H<sub>8,10</sub>N<sub>2</sub>O<sub>8,9</sub> and C<sub>5</sub>H<sub>9</sub>N<sub>3</sub>O<sub>10-12</sub> are the major 2N- and 3N-monomers. Their signal intensities are one to two  
438 orders of magnitude lower than those of 1N-monomers. According to the chemical composition, the 1N-  
439 monomers are likely to be the first-generation products from NO<sub>3</sub> oxidation of isoprene, while the 2N- and 3N-  
440 monomers probably arise from the further oxidation of 1N-monomers by NO<sub>3</sub>, which therefore should be  
441 second- or later-generation products. As mentioned before, the reaction of nitrooxy alkylperoxy radicals with  
442 NO<sub>2</sub> can lead to the formation of peroxy nitrates (for the special case peroxyacyl nitrates, PAN-like) containing  
443 two N atoms. The peroxy nitrates will decompose rapidly under experimental conditions, whereas the PAN-like  
444 compounds are more stable (with lifetimes ranging from minutes to weeks at 298K and ambient temperature).  
445 Such C<sub>5</sub> PAN-like compounds are isomers of aforementioned 2N-monomers, but ought to be first-generation  
446 products. In addition to C<sub>5</sub>-2N-monomers, we observe some C<sub>4</sub>-2N-monomers with relatively high intensity,  
447 such as C<sub>4</sub>H<sub>6</sub>N<sub>2</sub>O<sub>7</sub> at *m/z* 273 and C<sub>4</sub>H<sub>8</sub>N<sub>2</sub>O<sub>8</sub> at *m/z* 291. It is proposed that such C<sub>4</sub> dinitrates originate from the  
448 further oxidation of C<sub>5</sub> carbonyl compounds followed by unimolecular decomposition (Schwantes et al., 2015;  
449 Wennberg et al., 2018), as shown in Scheme S11.

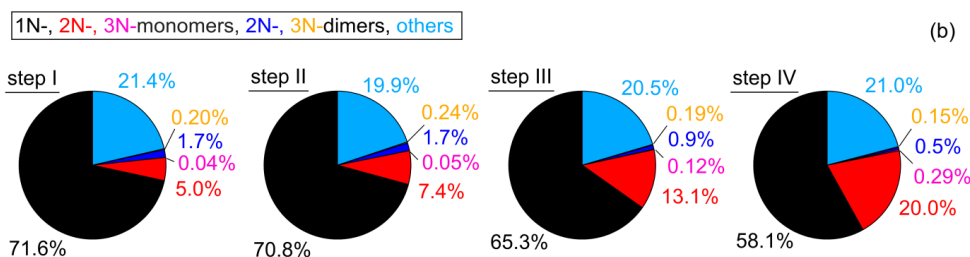
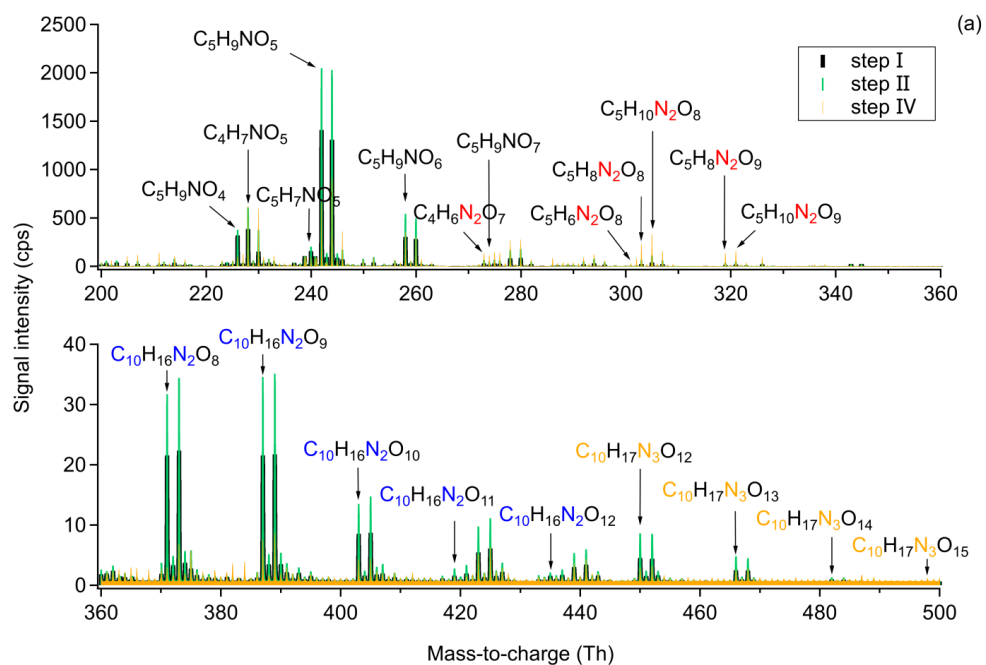
450 2N-Dimers are C<sub>10</sub> compounds with 8-12 oxygen atoms (C<sub>10</sub>H<sub>16</sub>N<sub>2</sub>O<sub>8-12</sub>), and their signal intensities are  
451 relatively low compared to that of monomers, approximately three orders of magnitude lower. They might be  
452 ROOR products from the self or cross reaction of two nitrooxy peroxy radicals (Berndt et al., 2018). 3N-Dimers  
453 are molecules consisting of 12–16 oxygen atoms (C<sub>10</sub>H<sub>17</sub>N<sub>3</sub>O<sub>12-16</sub>). They are probably formed from further  
454 oxidation of 2N-dimers or from the cross reaction of a nitrooxy peroxy radical with a dinitrooxy peroxy radicals.



455 **3.2 Multi-generation chemistry**

456 **3.2.1 Molecular composition for each step**

457 As mentioned in Sect. 2.2, there were four injections during the experiment on 8 August (denoted as step I, II,  
 458 III, IV in Fig. 3), wherein in the first three injections all components, O<sub>3</sub>, NO<sub>2</sub>, and isoprene, were added, while  
 459 in the last step only O<sub>3</sub> and NO<sub>2</sub> were injected to promote the further oxidation of early-generation products. The  
 460 extended oxidation time with reinjection of oxidants provides the opportunity to investigate the multi-generation  
 461 oxidation chemistry of isoprene-NO<sub>3</sub> system. The mass spectra show only slow changes in the concentrations  
 462 during the last period of each step, indicating weak chemical evolution. Therefore, we use integrated mass  
 463 spectra over the last 10 minutes of each step for further analysis. Due to the similarity of the integrated mass  
 464 spectra for step II and step III, the latter is omitted in Fig. 3.



465

466 **Figure 3: Comparison of the chemical composition of each oxidation step. (A) Averaged mass spectra for step I, II,**  
 467 **and IV, with the omitted spectrum of step III being very similar to that of step II. (B) Relative contribution of**  
 468 **different chemical groups for each oxidation step. Only organic products were counted for analysis. ‘Others’ refers to**  
 469 **CHO compounds without containing nitrogen atoms (e.g., C<sub>5</sub>H<sub>8</sub>O<sub>2</sub> and C<sub>5</sub>H<sub>8</sub>O<sub>3</sub>).**



470 As shown in Fig. 3a, large amounts of 1N-monomers were formed from  $\text{NO}_3$  oxidation of isoprene in step I,  
471 wherein  $\text{C}_5\text{H}_9\text{NO}_5$ ,  $\text{C}_5\text{H}_9\text{NO}_6$ , and  $\text{C}_4\text{H}_7\text{NO}_5$  are the most abundant compounds in signal. The 2N-monomers,  
472 which are expected from further oxidation of 1N-monomers, are much less compared to 1N-monomers,  
473 accounting for 5.0% of the total organic signals, with the 3N-monomers even less (0.04%). The low  
474 contributions of second-generation products probably results from the relatively high concentration of isoprene  
475 in step I, reducing the possibility for further oxidation of first-generation products. These results indicate that the  
476 system is dominated by first-generation chemistry at the early stage and therefore the oxidation state of products  
477 is low. In addition to monomers, some 2N- and 3N-dimers are observed. They contribute 1.7% and 0.2%,  
478 respectively, to the total organic signals, as shown in Fig. 3b. The low signal intensity of dimers probably results  
479 from their small yield under our experimental conditions. In this case their contribution to SOA formation might  
480 be small. However, a part of the dimers condense onto chamber wall due to their low volatility, so only a  
481 smaller portion exists in the gas phase (compare Table S3 and Fig. S6).

482 In step II, the secondary chemistry was accelerated by further addition of  $\text{O}_3$  and  $\text{NO}_2$ , but the primary  
483 chemistry was also maintained by isoprene injection. As a result, more 1N-monomers (e.g.  $\text{C}_5\text{H}_9\text{NO}_{4,5,6}$ ) were  
484 formed compared to step I, as well as dimers (e.g.,  $\text{C}_{10}\text{H}_{16}\text{N}_2\text{O}_{8,9,10}$  and  $\text{C}_{10}\text{H}_{17}\text{N}_3\text{O}_{12,13}$ ), as shown in Fig. 3a. The  
485 signals of 2N-monomers almost double in this period compared to those in step I, and their relative contribution  
486 increase from 5.0% to 7.4%. This is attributed to the further oxidation of first-generation products formed in  
487 step I. The relative contributions of different chemical groups exhibited in Fig. 3b clearly show that, although  
488  $\text{NO}_3$  produced from the second addition of  $\text{NO}_2$  and  $\text{O}_3$  still primarily reacted with newly-injected isoprene,  
489 reaction of  $\text{NO}_3$  with the first-generation oxidation products retaining a double bond was inevitable, leading to  
490 more second-generation 2N- or 3N-products compared to step I. The visibly increasing fraction of 2N-  
491 monomers indicates that the second-generation chemistry started to play a more important role than that in the  
492 early stage. In step III, the chemical process proceeded similarly, and thus is not further discussed here.

493 Due to the favorable conditions for further oxidation, the signals of 1N-monomers (such as  $\text{C}_3\text{H}_9\text{NO}_4$ ,  
494  $\text{C}_5\text{H}_9\text{NO}_5$ , and  $\text{C}_5\text{H}_9\text{NO}_6$ ), as well as 2N- and 3N-dimers, dropped dramatically in step IV, with their relative  
495 contributions decreasing to 58.1%, 0.5%, and 0.15%, respectively. The decrease in signals of dimers is primarily  
496 ascribed to lack of isoprene, as there were less peroxy radicals under this condition, and hence less dimers were  
497 formed. In addition, their condensation on the wall and dilution also contributed to the decreasing signals.  
498 Furthermore, dimers with 2 or 3 nitrogen atoms possess at least one double bond in their molecular structures  
499 and can thus be further oxidized under high  $\text{NO}_3$  condition to form 4N- or 5N-dimers. However, only few 4N-  
500 dimers and no 5N-dimers were detected by CIMS, suggesting that the 4N- and 5N-dimers were either not  
501 formed, or condensed on the wall due to their low volatilities. In contrast, 2N- and 3N-monomers increase  
502 significantly, with their relative contributions ascending to 20.0% and 0.29%, respectively. This indicates that  
503 2N- and 3N-monomers might be second- or later-generation products that are formed from the further oxidation  
504 of first-generation products. Additionally, unlike the  $\text{C}_5$  monomers, the signal of  $\text{C}_4\text{H}_7\text{NO}_5$  increased in step IV,  
505 indicating that there is a new formation pathway for  $\text{C}_4\text{H}_7\text{NO}_5$  under excess  $\text{NO}_3$  condition. No double bond can  
506 remain in such products, as otherwise they would be oxidized and their signal should decay instead.

507 In summary, above findings confirm that multi-generation chemistry happened during the  $\text{NO}_3$ -initiated  
508 isoprene oxidation, and that the later generation oxidation was promoted by “excess”  $\text{NO}_3$  radicals.





### 509 3.2.2 Carbon oxidation state ( $\overline{OS}_C$ )

510 The oxidation state of carbon ( $\overline{OS}_C$ ) is defined as the charge a carbon atom takes with assumption that it loses  
511 completely all electrons in bonds to more electronegative atoms and vice versa (Kroll et al., 2011). This quantity  
512 is a metric for the degree of oxidation and will increase with oxidation. Moreover,  $\overline{OS}_C$  together with carbon  
513 number can be used to constrain the composition of organic mixtures and provide insights into their evolutions.  
514 The carbon oxidation state of a species is determined by the relative abundances and oxidation states of non-  
515 carbon atoms in the compound. Since we observed nitrate groups in the products,  $\overline{OS}_C$  is defined by Eq. (3). In  
516 this study, the group-averaged  $\overline{OS}_C$  is the signal-weighted mean average carbon oxidation state of compounds  
517 with the same carbon number, and the bulk-averaged  $\overline{OS}_C$  is the signal-weighted mean average carbon oxidation  
518 state of all detected compounds in the system.

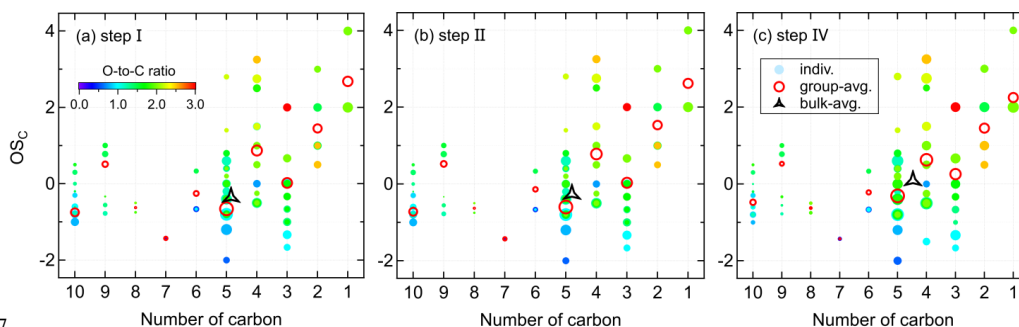
$$519 \quad \overline{OS}_C = \frac{2 \times n_O - n_H - 5 \times n_N}{n_C} \quad (3)$$

520 wherein,  $n_O$ ,  $n_H$ , and  $n_N$  are the number of the respective atoms in the molecular formula.

521 Figure 4 shows the distribution of gas-phase products from the isoprene- $\text{NO}_3$  system in the oxidation state  
522 versus carbon number ( $OS_C$  vs  $n_C$ ) space. The bulk-averaged  $\overline{OS}_C$  is -0.35 in step I, wherein the smaller  
523 molecules ( $C_{\leq 4}$ ) have higher oxidation states than the larger molecules. The group-averaged oxidation state of  
524  $C_5$  compounds is relatively low ( $\overline{OS}_{C=5} = -0.66$ ), indicating that both of the oxidation and autoxidation degree of  
525 isoprene are quite low during this period. This is consistent with the conclusion made previously from mass  
526 spectra results that at the early stage isoprene- $\text{NO}_3$  oxidation was dominated by first-generation chemistry.

527 The system  $\overline{OS}_C$  increases to -0.26 in step II, confirming that first-generation products were further  
528 oxidized after the second injection. During this step, the  $\overline{OS}_C$  of most compound groups increase only weakly,  
529 except for that of the  $C_5$  compounds. The group-averaged  $\overline{OS}_C$  of  $C_5$  compounds increases to -0.60 in step II,  
530 which is the major contributor to the increase of  $\overline{OS}_C$  of the whole system. The increase of  $\overline{OS}_C$  of  $C_5$   
531 compounds is largely attributed to the formation of 2N-monomers expected from further oxidation of existing  
532 1N-products formed in step I. This is confirmed by the detectable increase of 2N- and 3N-monomers in the mass  
533 spectra and their higher relative contributions to total signals (see Fig. 3). In addition to  $C_5$  compounds, the  $\overline{OS}_C$   
534 of  $C_3$  and  $C_6$  products increase significantly in step II.

535 In step IV, the secondary oxidation was largely accelerated by reinjection of  $\text{O}_3$  and  $\text{NO}_2$ , and hence the  
536 system oxidation degree increases, with the bulk-averaged  $\overline{OS}_C$  growing substantially to 0.09. Similarly, the  
537 significant increase of system  $\overline{OS}_C$  is mainly attributed to the  $C_5$  compounds, with their group-averaged  $\overline{OS}_C$   
538 increasing to -0.31. In addition, the  $\overline{OS}_C$  of  $C_{10}$  compounds increased evidently despite their decreasing signals,  
539 suggesting  $C_{10}$  dimers were further oxidized as well in step IV. It is worth noting that the average carbon  
540 number decreases step by step with increasing  $\overline{OS}_C$ . This is the case because fewer  $C_{10}$  products, but more  
541 fragments were formed with the reaction proceeding, as shown in Fig.4 by the decreasing peak areas of larger  
542 molecules but converse trend for smaller molecules. One conceivable explanation for the decreasing dimers but  
543 increasing fragments with the increasing  $\overline{OS}_C$  is that, with more highly oxidized  $\text{RO}_2$  formed under high  $\text{NO}_3$   
544 condition, the prevailing fate of  $\text{RO}_2$  changes from dimerization to forming alkoxy radicals, which would  
545 undergo unimolecular decomposition rapidly, especially when there is a neighboring oxygen-containing  
546 functional group (Molteni et al., 2019).



547

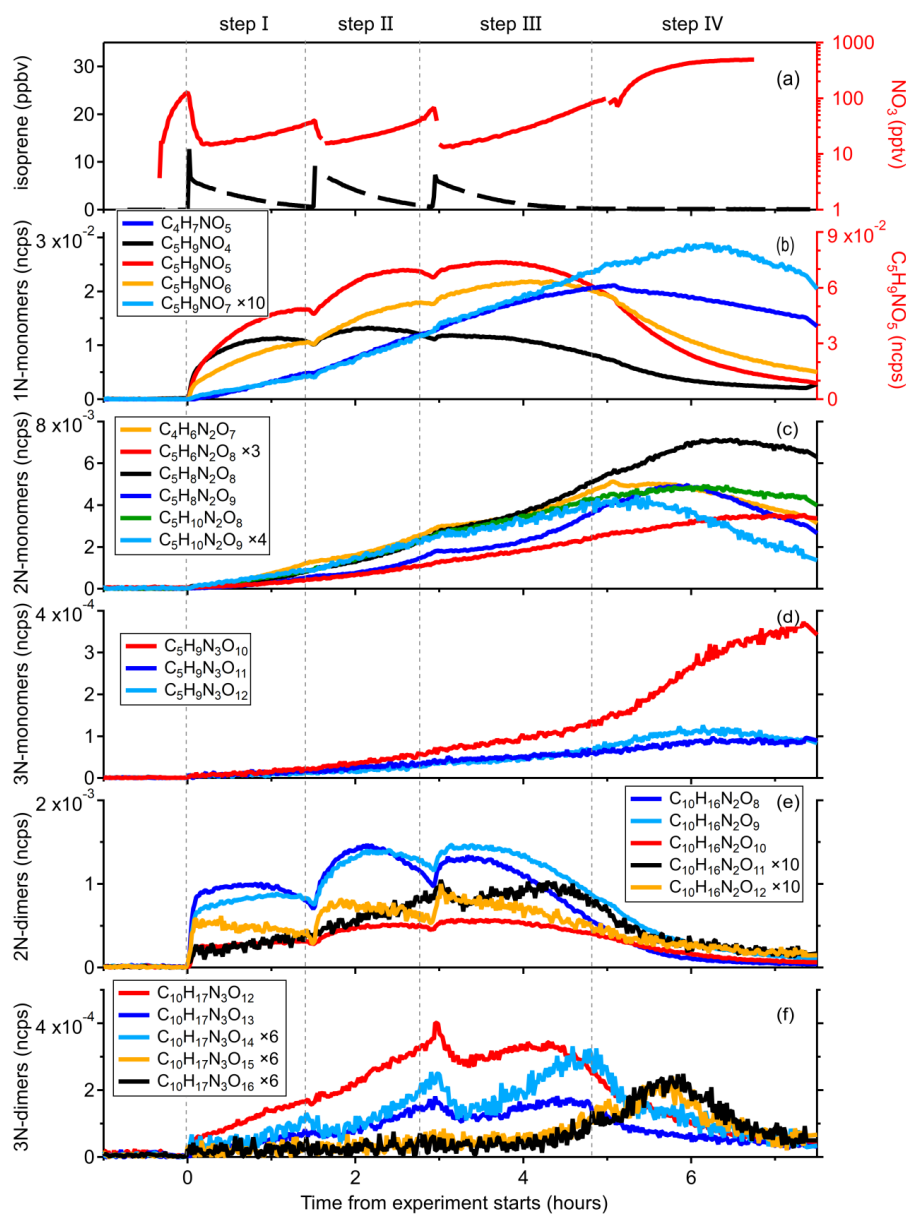
548 **Figure 4: Distribution of gas-phase products from isoprene oxidation by  $\text{NO}_3$  in the carbon oxidation state ( $\overline{OS}_C$ )**  
549 **versus carbon number ( $nc$ ) space. Markers are colored by oxygen-to-carbon molar ratio and sized by the logarithm**  
550 **of peak areas. The group-averaged and bulk-averaged  $\overline{OS}_C$  are signal-weighted mean average carbon oxidation state**  
551 **of compounds with the same carbon number and of all detected compounds, respectively.**

552 In summary, isoprene and its products undergo further oxidation by  $\text{NO}_3$ , leading to an increase in degree  
553 of oxidation of products as the reaction proceeds. The increasing bulk  $\overline{OS}_C$  is largely governed by the highly  
554 oxidized  $\text{C}_5$  compounds. In addition, more fragments but fewer dimers are formed as the  $\overline{OS}_C$  increases, which  
555 can be probably explained by the change of  $\text{RO}_2$  fate from prevailing dimerization to fragmentation through the  
556 alkoxy radical channel.

### 557 3.2.3 Characteristics of different-generation products

#### 558 (1) 1N-monomers

559 To illustrate the multi-generation chemistry involved in the isoprene- $\text{NO}_3$  reaction system, Fig. 5 shows the time  
560 evolution of the major gas-phase products. The signal of the most abundant compounds,  $\text{C}_5\text{H}_9\text{NO}_5$ , increases  
561 rapidly as soon as the reaction was initiated, reaching a maximum when its chemical production rate matches its  
562 loss rate (including chemical destruction, wall loss, dilution, etc.), and decreases slowly thereafter. Its time  
563 behavior in the first three steps is similar. In step IV, however, the injection of  $\text{O}_3$  and  $\text{NO}_2$  resulted in a strong  
564 decay of  $\text{C}_5\text{H}_9\text{NO}_5$ , owing to the occurrence of further oxidation by  $\text{NO}_3$ . The time behavior suggests that  
565  $\text{C}_5\text{H}_9\text{NO}_5$  signal is dominated by first-generation oxidation products, and the same conclusion can be made for  
566  $\text{C}_5\text{H}_9\text{NO}_4$  and  $\text{C}_5\text{H}_9\text{NO}_6$ . According to the mechanistic framework developed above, the  $\text{C}_5\text{H}_9\text{NO}_4$ ,  $\text{C}_5\text{H}_9\text{NO}_5$ ,  
567 and  $\text{C}_5\text{H}_9\text{NO}_6$  compounds most likely correspond to hydroxyl nitrates, nitroxy hydroperoxides, and hydroxy  
568 hydroperoxy nitrates, respectively, but other constitutional isomers are possible. They were already observed in  
569 previous studies and were proposed to form through reactions of  $\text{INO}_2$  radicals with  $\text{RO}_2$ ,  $\text{HO}_2$ , and  
570 unimolecular rearrangement, as shown in Scheme S5 (Ng et al., 2008; Kwan et al., 2012; Schwantes et al., 2015;  
571 Wennberg et al., 2018).



572

573 **Figure 5: Time evolution of selected gas-phase compounds measured during the isoprene - NO<sub>3</sub> experiment on 08**  
574 **August, 2018. (a) Time series of O<sub>3</sub>, NO<sub>2</sub>, NO<sub>3</sub> and isoprene. (b)–(f) Time evolution of major 1N-monomers (C<sub>5</sub>H<sub>9</sub>NO<sub>4</sub>–**  
575 **7 and C<sub>4</sub>H<sub>7</sub>NO<sub>5</sub>), 2N-monomers (C<sub>4</sub>H<sub>6</sub>N<sub>2</sub>O<sub>7</sub>, C<sub>5</sub>H<sub>8</sub>N<sub>2</sub>O<sub>8</sub>, and C<sub>5</sub>H<sub>8,10</sub>N<sub>2</sub>O<sub>8,9</sub>), 3N-monomers (C<sub>5</sub>H<sub>9</sub>N<sub>3</sub>O<sub>10–12</sub>), 2N-dimers**  
576 **(C<sub>10</sub>H<sub>16</sub>N<sub>2</sub>O<sub>8–12</sub>), and 3N-dimers (C<sub>10</sub>H<sub>17</sub>N<sub>3</sub>O<sub>12–16</sub>).**

577

As shown in Fig. 5b, the temporal evolution of C<sub>5</sub>H<sub>9</sub>NO<sub>7</sub> (*m/z* 274) is different to C<sub>5</sub>H<sub>9</sub>NO<sub>4–6</sub> compounds,  
suggesting that it has a completely different formation pathway. Specifically, the formation rate of C<sub>5</sub>H<sub>9</sub>NO<sub>7</sub> is  
initially much slower than that of C<sub>5</sub>H<sub>9</sub>NO<sub>4–6</sub> but accelerates to become comparable to them later as the  
experiment proceeds, i.e. when a multitude of first-generation products are accumulated. This implies that

580



581  $C_5H_9NO_7$  is produced from the further oxidation of first-generation products, and its signal is dominated by  
582 second-generation products. Based on its molecular composition,  $C_5H_9NO_7$  could be the dihydroperoxy nitrate  
583 as shown in Scheme S5, but its formation through the reaction of  $HO_2$  with nitrooxy hydroperoxy radical from  
584  $INO_2$  autoxidation suggests it should be first-generation products, not in accordance with the time behavior we  
585 actually observe. Consequently, we can conclude that it is not the major formation pathway that contributed to  
586  $C_5H_9NO_7$  observed in this study. As shown in Scheme S7, the first-generation  $C_5$  hydroxy carbonyl ( $C_5H_8O_2$ ,  
587  $m/z$  179) can be further oxidized by  $NO_3$  and the resulting alkyl radical would rapidly recombine with  $O_2$ ,  
588 producing a new peroxy radical, which then reacts with  $HO_2$  radicals to form  $C_5H_9NO_7$  (hydroxy hydroperoxy  
589 carbonyl nitrate). Similarly, the  $C_5$  hydroperoxy carbonyl ( $C_5H_8O_3$ ,  $m/z$  195) can also lead to the formation of  
590 such  $C_5H_9NO_7$  (isomer of that formed through  $C_5H_8O_2$  channel) through further oxidation (see Scheme S7).  
591 According to above two mechanisms,  $C_5H_9NO_7$  formed following such reaction pathways should be second-  
592 generation products, better consistent with its time behavior.

593 Considering its similar time behavior to  $C_5H_9NO_7$ , the observed  $C_4H_7NO_5$  ( $m/z$  228) signal is likewise  
594 thought to be dominated by second-generation products. Schwantes et al. (2015) proposed such a  $C_4$  product  
595 based on OH-initiated chemistry, but as the OH concentration in our system was close to zero during the  
596 experiment (see Fig. S3), this formation pathway cannot apply in our situation. Instead, we suggest that  
597  $C_4H_7NO_5$  is formed through the unimolecular decomposition of the  $C_5$  alkoxy or acyl radicals, which result from  
598 further oxidation of the  $C_5$  hydroxy carbonyl ( $C_5H_8O_2$ ,  $m/z$  179), as shown in Scheme S7. It should be pointed  
599 out here that there may be reaction pathways forming  $C_4H_7NO_5$  as first-generation products that are not  
600 considered here, whereas it is no doubt that the second-generation chemistry played a dominant role in  $C_4H_7NO_5$   
601 formation according to its time evolution measured by CIMS.

602 Although  $C_4H_7NO_5$  and  $C_5H_9NO_7$  show similar time behaviors in the first three steps, it seems that they  
603 followed fairly different reaction pathways when the concentration of  $NO_3$  in the chamber increased  
604 dramatically in step IV. As shown in Fig. 5b, the signal of  $C_4H_7NO_5$  drops immediately after the injection of  $O_3$   
605 and  $NO_2$ , while that of  $C_5H_9NO_7$  continues to increase, although its formation rate becomes slightly lower with  
606 increasing  $NO_3$  concentration. The decay of  $C_4H_7NO_5$  signal can be explained by more chemical destruction or  
607 less production under high  $NO_3$  condition, wherein the latter seems more sensible in terms of its structure (no  
608 double bond remaining). As shown in Scheme S7, the second-generation  $C_4H_7NO_5$  and  $C_5H_9NO_7$  compounds  
609 share the same precursor in the  $C_5H_8O_2$  channel. Consequently, the production of  $C_5H_9NO_7$  through this  
610 pathway would be interrupted immediately after the injection of  $O_3$  and  $NO_2$  like  $C_4H_7NO_5$ . In reality, its signal  
611 might decay even faster due to the larger reaction rate of  $RO_2$  H-shift (leading to the formation of  $C_4H_7NO_5$ )  
612 than that of  $RO_2$  reacting with  $HO_2$  (leading to the formation of  $C_5H_9NO_7$ ). As presented by Vereecken and  
613 Nozière (2020), the rate coefficient of aldehydic H-shift is  $\geq 0.5 \text{ s}^{-1}$  (298 K), while the pseudo first order rate  
614 coefficient of  $RO_2$  reacting with  $HO_2$  is  $\sim 10^{-3} \text{ s}^{-1}$  ( $k$  (298 K) =  $5 \times 10^{-12} \text{ cm}^3 \text{ molecules}^{-1} \text{ s}^{-1}$  (Atkinson, 2007), and  
615  $[HO_2] \sim 4 \times 10^8 \text{ molecules cm}^{-3}$ ), about two orders of magnitude smaller. This result implies that the increasing  
616  $C_5H_9NO_7$  observed is contributed to by other formation pathways. As mentioned before,  $C_5H_9NO_7$  can also be  
617 produced by  $C_5H_8O_3$  oxidation. We find that the signal of  $C_4H_7NO_6$  ( $m/z$  244), which results from  $C_5H_8O_3$   
618 oxidation as well, remains increasing after the injection of  $O_3$  and  $NO_2$ . This tentatively confirms that the  
619 production of  $C_5H_9NO_7$  in step IV is mainly from  $C_5H_8O_3$  oxidation channel. More experimental or theoretical  
620 studies are needed to provide insights into these differences.



621 **(2) 2N- and 3N-monomers**

622 As shown in Fig. 5c, 2N-monomers formed much slower than 1N-monomers in the early stage, but their  
623 formation rates were accelerated in step II and step III, probably due to the accumulation of first-generation  
624 products. According to our mechanistic framework, 2N-monomers are second-generation products resulting  
625 from the further oxidation of 1N-monomers by  $\text{NO}_3$ , which is consistent with their time behaviors detected by  
626 CIMS.

627 Like  $\text{C}_4\text{H}_7\text{NO}_5$  and  $\text{C}_5\text{H}_9\text{NO}_7$ , different 2N-monomers have similar behavior in the first three steps, but they  
628 are obviously different in step IV when the concentration of  $\text{NO}_3$  increased drastically in the chamber. For  
629 instance, the signals of  $\text{C}_5\text{H}_8\text{N}_2\text{O}_8$ ,  $\text{C}_5\text{H}_8\text{N}_2\text{O}_9$  and  $\text{C}_5\text{H}_{10}\text{N}_2\text{O}_8$  continue to increase after the injection of  $\text{O}_3$  and  
630  $\text{NO}_2$ , while that of  $\text{C}_5\text{H}_{10}\text{N}_2\text{O}_9$  drops immediately. This is related to their detailed formation mechanisms which  
631 are outside the scope of this study. Furthermore,  $\text{C}_5\text{H}_8\text{N}_2\text{O}_9$  and  $\text{C}_5\text{H}_{10}\text{N}_2\text{O}_9$  decay a little bit faster than  
632  $\text{C}_5\text{H}_8\text{N}_2\text{O}_8$  and  $\text{C}_5\text{H}_{10}\text{N}_2\text{O}_8$ , which might be related to their volatility and will be further discussed in next section.

633 Different from other 2N-monomers, the signals of  $\text{C}_5\text{H}_6\text{N}_2\text{O}_8$  ( $m/z$  301) increases continuously under high  
634  $\text{NO}_3$  condition, although its net formation rate is almost zero at the end of step IV. The characteristics of  
635  $\text{C}_5\text{H}_6\text{N}_2\text{O}_8$  under high  $\text{NO}_3$  condition reflects its different formation pathways from other dinitrates, and without  
636 having a comprehensive knowledge of its chemical mechanism, we are unable to tell what exactly leads to the  
637 differences. In the Master Chemical Mechanism (MCM v3.3.1),  $\text{C}_5\text{H}_6\text{N}_2\text{O}_8$  is proposed to be a PAN-like  
638 compound stemming from the  $\text{C}_5$  nitrooxy carbonyl ( $\text{C}_5\text{H}_7\text{NO}_4$ )  
639 (<http://mcm.leeds.ac.uk/MCM/browse.htm?species=NC4CHO>). Such  $\text{C}_5\text{H}_6\text{N}_2\text{O}_8$  compound would react with  
640  $\text{NO}_3$  radicals due to the remaining double bond, and hence this cannot be the predominant formation pathway of  
641 the  $\text{C}_5\text{H}_6\text{N}_2\text{O}_8$  observed in this study. Based on the formation mechanism of dinitrooxyepoxides ( $\text{C}_5\text{H}_8\text{N}_2\text{O}_7$ )  
642 proposed by Kwan et al. (2012), we suggest that  $\text{C}_5\text{H}_6\text{N}_2\text{O}_8$  can also be a dinitrooxyepoxide resulting from  
643 cyclization of specific hydroperoxy alkyl radicals, as shown in Scheme S10. Alternatively, the  $\text{C}_5$  hydroxy  
644 nitrate ( $\text{C}_5\text{H}_9\text{NO}_4$ ) can be oxidized by  $\text{NO}_3$  and then react with  $\text{NO}_3$  radicals again, forming  $\text{C}_5\text{H}_6\text{N}_2\text{O}_8$  with two  
645 aldehyde groups ultimately (see Scheme S10). According to the proposed mechanisms above,  $\text{C}_5\text{H}_6\text{N}_2\text{O}_8$  formed  
646 through the first two pathways are second-generation products, while those from the third channel are third-  
647 generation products, in accordance with its time behavior measured by CIMS.

648 In addition to  $\text{C}_5$ -2N-monomers, we observe some  $\text{C}_4$  dinitrates such as  $\text{C}_4\text{H}_6\text{N}_2\text{O}_7$  ( $m/z$  273) and  $\text{C}_4\text{H}_8\text{N}_2\text{O}_8$   
649 ( $m/z$  291), and the signal intensity of  $\text{C}_4\text{H}_6\text{N}_2\text{O}_7$  is comparable to the major  $\text{C}_5$ -2N-monomers.  $\text{C}_4$  dinitrates have  
650 rarely been mentioned in previous isoprene- $\text{NO}_3$  studies. As shown in Fig. 5c,  $\text{C}_4\text{H}_6\text{N}_2\text{O}_7$  has similar time  
651 behavior to  $\text{C}_5$ -2N-monomers, and hence is thought to be second-generation products. Wennberg et al. (2018)  
652 proposed that such a  $\text{C}_4$  dinitrate was generated from OH-initiated further oxidation of  $\text{C}_5\text{H}_7\text{NO}_4$ . However, this  
653 is not applicable here due to a lack of OH radicals in our system. Instead, we propose that the  $\text{C}_4\text{H}_6\text{N}_2\text{O}_7$   
654 observed in this study is dinitrooxy carbonyl compound resulting from  $\text{NO}_3$  oxidation of  $\text{C}_5\text{H}_7\text{NO}_4$  with  
655 subsequent unimolecular decomposition (see Scheme S11 for details).

656 As shown in Fig. 5d, 3N-monomers are generated more slowly than 1N-monomers, but their signals grow  
657 gradually as the experiment proceeds, with a significant increase especially for  $\text{C}_5\text{H}_9\text{N}_3\text{O}_{10}$  in the last step.  
658 Furthermore, we can see from Fig. 5c and Fig. 5d that the signals of  $\text{C}_5$  trinitrates in step IV appear  
659 anticorrelated to that of  $\text{C}_5\text{H}_{10}\text{N}_2\text{O}_8$  and  $\text{C}_5\text{H}_{10}\text{N}_2\text{O}_8$ . The gas-phase 3N-monomers have rarely been reported in  
660 previous literature. Ng et al. (2008) observed  $\text{C}_5\text{H}_9\text{N}_3\text{O}_{10}$  compound in the particle-phase and assumed that it



661 was produced from  $\text{NO}_3$  oxidation of the  $\text{C}_5$  hydroxy nitrate ( $\text{C}_5\text{H}_9\text{NO}_4$ ). Similarly,  $\text{C}_5\text{H}_9\text{N}_3\text{O}_{11}$  and  $\text{C}_5\text{H}_9\text{N}_3\text{O}_{12}$   
662 can be formed through  $\text{NO}_3$  reacting with dinitrooxy peroxy radicals, which result from corresponding first-  
663 generation nitrooxy compounds ( $\text{C}_5$  hydroperoxy nitrate,  $\text{C}_5\text{H}_9\text{NO}_5$  or  $\text{C}_5$  hydroxy hydroperoxy nitrate,  $\text{C}_5\text{H}_9\text{NO}_6$ )  
664 oxidation by  $\text{NO}_3$  radicals, as shown in Scheme S12. 3N-Monomers formed following such pathways are  
665 second-generation products by definition. Regarding the rising signals of 3N-monomers in step IV, one  
666 explanation is that although the reaction of dinitrooxy peroxy radicals with  $\text{NO}_3$  is not an oxidation process,  
667 their formation can be significantly facilitated by increasing  $\text{NO}_3$  concentration. It is also possible that 3N-  
668 monomers are formed through H-abstraction of 2N-monomers.  $\text{NO}_3$  radicals can abstract the hydrogen of  
669 dihydroxy dinitrate ( $\text{C}_5\text{H}_{10}\text{N}_2\text{O}_8$ ) or hydroxyl hydroperoxy dinitrate ( $\text{C}_5\text{H}_{10}\text{N}_2\text{O}_9$ ) from the carbon with an  $-\text{OH}$ ,  
670  $-\text{OOH}$  or  $-\text{ONO}_2$  group attached, leading to alkyl radicals that can subsequently recombine with  $\text{O}_2$  and then  
671 react with  $\text{NO}_2$  or  $\text{NO}_3$ , yielding trinitrates or peroxytrinitrates containing three nitrogen atoms. 3N-Monomers  
672 stemming from such reactions ought to be third-generation products. However, we should point out that 3N-  
673 monomers formed following H-abstraction pathway are less likely because abstracting hydrogen from the  
674 hydroxyl, hydroperoxy or nitrooxy carbon would lead to fragmentation at most cases (Bianchi et al., 2019).

675 In addition, it is interesting to note that the signal of  $\text{C}_5\text{H}_9\text{N}_3\text{O}_{10}$  increases continuously throughout step IV,  
676 whereas that of  $\text{C}_5\text{H}_9\text{N}_3\text{O}_{11}$  and  $\text{C}_5\text{H}_9\text{N}_3\text{O}_{12}$  drop after a short period of growth. Meanwhile, the production of  
677  $\text{C}_5\text{H}_9\text{N}_3\text{O}_{10}$  is facilitated by the increasing  $\text{NO}_3$  concentration compared to that of  $\text{C}_5\text{H}_9\text{N}_3\text{O}_{12}$  and  $\text{C}_5\text{H}_9\text{N}_3\text{O}_{11}$ .  
678 Currently, we cannot explain what exactly causes these differences, but we suspect that there may be different  
679 chemical pathways forming different 3N-monomers that are not covered here and may also be related to their  
680 different physical properties, such as vapor pressures.

### 681 (3) 2N- and 3N-dimers

682 As shown in Fig. 5e, 2N-dimers (except for  $\text{C}_{10}\text{H}_{16}\text{N}_2\text{O}_{11}$ ) display very similar time behavior to 1N-monomer,  
683 which form rapidly after each injection, indicating that the signals of 2N-dimers are dominated by first-  
684 generation products like most 1N-monomers. It is noted that the time behavior of  $\text{C}_{10}\text{H}_{16}\text{N}_2\text{O}_{11}$  ( $m/z$  419) is  
685 completely different from that of other 2N-dimers. As illustrated in Fig. 5e, the production rate of  $\text{C}_{10}\text{H}_{16}\text{N}_2\text{O}_{11}$   
686 is initially much slower compared to other dimers. Besides, its signal increases monotonically in the first two  
687 oxidation stages, whereas that of the others always increase first, approaching the maximum as its chemical  
688 production competes against the losses, and decrease gradually thereafter. The special time behavior of  
689  $\text{C}_{10}\text{H}_{16}\text{N}_2\text{O}_{11}$  suggests that it has a different formation pathway from other 2N-dimers, and its signal is most  
690 likely dominated by secondary products. In addition, we find that the signal of  $\text{C}_{10}\text{H}_{16}\text{N}_2\text{O}_{12}$  always starts to  
691 decay earlier than that of  $\text{C}_{10}\text{H}_{16}\text{N}_2\text{O}_8$  and  $\text{C}_{10}\text{H}_{16}\text{N}_2\text{O}_9$ . If we assume that their production rates have the same  
692 order of magnitude (confirming by their formation rates after each injection), then it can be concluded that  
693  $\text{C}_{10}\text{H}_{16}\text{N}_2\text{O}_{12}$  had additional chemical destruction, or its volatility is much lower than  $\text{C}_{10}\text{H}_{16}\text{N}_2\text{O}_8$  and  
694  $\text{C}_{10}\text{H}_{16}\text{N}_2\text{O}_9$  and hence has more rapid lost on the wall. It seems the second hypothesis is more likely when  
695 comparing its signal with and without dilution and wall-loss corrections (see Fig. S4). More detailed discussion  
696 about volatilities of different isoprene organonitrates will be provided in the next section.

697 It is proposed that dimers ( $\text{ROOR}'$ ) are likely formed through the self- or cross-reaction of two peroxy  
698 radicals (Berndt et al. 2018). Consequently, the generation number of dimers depends only on how the involved  
699 peroxy radicals are formed. Table S1 summarizes the possible permutation scheme of 2N-dimers from  $\text{RO}_2 +$



700 RO<sub>2</sub> reactions, and their structural information can be found in Scheme S13. For example, self-reaction of two  
701 C<sub>5</sub> nitrooxy peroxy radicals (C<sub>5</sub>H<sub>8</sub>NO<sub>5</sub>) leads to the formation of C<sub>10</sub>H<sub>16</sub>N<sub>2</sub>O<sub>8</sub> compound, while recombination  
702 of two C<sub>5</sub> nitrooxy hydroxyl peroxy radicals (C<sub>5</sub>H<sub>8</sub>NO<sub>6</sub>) or a C<sub>5</sub> nitrooxy peroxy radical (C<sub>5</sub>H<sub>8</sub>NO<sub>5</sub>) with a C<sub>5</sub>  
703 nitrooxy hydroperoxy peroxy radical (C<sub>5</sub>H<sub>8</sub>NO<sub>7</sub>) results in C<sub>10</sub>H<sub>16</sub>N<sub>2</sub>O<sub>10</sub> compound. According to their time  
704 behavior, 2N-dimers (except for C<sub>10</sub>H<sub>16</sub>N<sub>2</sub>O<sub>11</sub>) are thought to be first-generation products, and from this fact we  
705 can infer that the peroxy radicals contributing to dimer formation are dominated by first-generation  
706 intermediates. With regard to C<sub>10</sub>H<sub>16</sub>N<sub>2</sub>O<sub>11</sub>, we conclude that it is most likely a secondary product considering  
707 its typical second-generation behavior. In other words, at least one of the two C<sub>5</sub> nitrooxy peroxy radicals  
708 involved in formation of C<sub>10</sub>H<sub>16</sub>N<sub>2</sub>O<sub>11</sub> must be a secondary intermediate. As listed in Table S1, C<sub>10</sub>H<sub>16</sub>N<sub>2</sub>O<sub>11</sub> can  
709 be formed through C<sub>5</sub>H<sub>8</sub>NO<sub>6</sub> + C<sub>5</sub>H<sub>8</sub>NO<sub>7</sub> or C<sub>5</sub>H<sub>8</sub>NO<sub>6</sub> + C<sub>5</sub>H<sub>8</sub>NO<sub>7</sub> reactions, wherein C<sub>5</sub>H<sub>8</sub>NO<sub>7</sub> and C<sub>5</sub>H<sub>8</sub>NO<sub>8</sub>  
710 would be secondary peroxy radicals if they are formed through NO<sub>3</sub> further oxidation of the C<sub>5</sub> hydroxy  
711 carbonyl compounds (C<sub>5</sub>H<sub>8</sub>O<sub>2</sub> or C<sub>5</sub>H<sub>8</sub>O<sub>3</sub>), as shown in Scheme S7. In addition, it is possible that C<sub>10</sub>H<sub>16</sub>N<sub>2</sub>O<sub>11</sub> is  
712 formed from a C<sub>5</sub> hydroxy peroxy radical C<sub>5</sub>H<sub>9</sub>O<sub>3</sub> reacting with a C<sub>5</sub> dinitrooxy hydroxy carbonyl peroxy radical  
713 C<sub>5</sub>H<sub>7</sub>N<sub>2</sub>O<sub>10</sub> (from C<sub>5</sub>H<sub>7</sub>NO<sub>5</sub> oxidation by NO<sub>3</sub>), as we observe high abundant C<sub>5</sub>H<sub>10</sub>O<sub>3</sub> during the experiment,  
714 although C<sub>5</sub>H<sub>10</sub>O<sub>3</sub> is assumed to be the major product of the OH-initiated chemistry.

715 Apart from 2N-dimers, we observe detectable signals at *m/z* 450, 466, 482, 498 and 514, which are  
716 identified as 3N-dimers with molecular formulas C<sub>10</sub>H<sub>17</sub>N<sub>3</sub>O<sub>12-16</sub>. C<sub>10</sub>H<sub>17</sub>N<sub>3</sub>O<sub>12</sub> and C<sub>10</sub>H<sub>17</sub>N<sub>3</sub>O<sub>13</sub> were detected  
717 in the particle-phase in previous study, suggesting that they have low volatility and can contribute to SOA  
718 formation (Ng et al., 2008). As shown in Fig. 5f, 3N-dimers form much slower than 2N-dimers, but their  
719 productions are accelerated as the experiment proceeds. This is similar to the characteristics of second-  
720 generation 2N- and 3N-monomers to some degree, suggesting that the signals of 3N-dimers we observed are  
721 most likely dominated by secondary or even later-generation compounds.

722 It is worth noting that C<sub>10</sub>H<sub>17</sub>N<sub>3</sub>O<sub>12-14</sub> and C<sub>10</sub>H<sub>17</sub>N<sub>3</sub>O<sub>15,16</sub> have two completely different types of time  
723 behavior. The signals of C<sub>10</sub>H<sub>17</sub>N<sub>3</sub>O<sub>12</sub>, C<sub>10</sub>H<sub>17</sub>N<sub>3</sub>O<sub>13</sub> and C<sub>10</sub>H<sub>17</sub>N<sub>3</sub>O<sub>14</sub> more or less increase in the first three  
724 oxidation steps and start to decline in the late of step III with increasing NO<sub>3</sub> concentration. As depicted in  
725 Scheme S13, 3N-dimers can result from further oxidation of 2N-dimers or the cross-reaction of a first-  
726 generation nitrooxy peroxy radical with a secondary dinitrooxy peroxy radical. Accordingly, such 3N-dimers are  
727 thought to be second-generation products, and they would further react with NO<sub>3</sub> due to the remaining double  
728 bond in their molecular structure, leading to severe chemical destruction of these compounds under high NO<sub>3</sub>  
729 condition. This is consistent with the time behavior of C<sub>10</sub>H<sub>17</sub>N<sub>3</sub>O<sub>12</sub>, C<sub>10</sub>H<sub>17</sub>N<sub>3</sub>O<sub>13</sub> and C<sub>10</sub>H<sub>17</sub>N<sub>3</sub>O<sub>14</sub>. In contrast,  
730 C<sub>10</sub>H<sub>17</sub>N<sub>3</sub>O<sub>15</sub> and C<sub>10</sub>H<sub>17</sub>N<sub>3</sub>O<sub>16</sub> are formed even more slowly, and their production in the first four hours is close  
731 to zero. However, their signals start to climb in the late of step III, during which that of C<sub>10</sub>H<sub>17</sub>N<sub>3</sub>O<sub>12</sub>,  
732 C<sub>10</sub>H<sub>17</sub>N<sub>3</sub>O<sub>13</sub> and C<sub>10</sub>H<sub>17</sub>N<sub>3</sub>O<sub>14</sub> decline. This suggests that C<sub>10</sub>H<sub>17</sub>N<sub>3</sub>O<sub>15</sub> and C<sub>10</sub>H<sub>17</sub>N<sub>3</sub>O<sub>16</sub> formed under high NO<sub>3</sub>  
733 condition probably result from further reactions of C<sub>10</sub>H<sub>17</sub>N<sub>3</sub>O<sub>12-14</sub>. However, this assumption is highly uncertain  
734 and more experimental and theoretical studies are needed to substantiate it. In terms of their time behavior,  
735 C<sub>10</sub>H<sub>17</sub>N<sub>3</sub>O<sub>15</sub> and C<sub>10</sub>H<sub>17</sub>N<sub>3</sub>O<sub>16</sub> are thought to be third- or even later-generation products.



736 **3.3 Volatility distribution of isoprene nitrates**

737 **3.3.1 C\* estimated by experimental methods**

738 Detailed information about the volatility of organic molecules is essential to evaluate their potential to form  
739 SOA. In order to investigate the potential contribution of various isoprene oxidation products to SOA formation,  
740 we use our (limited) experimental data to estimate the vapor pressure of different isoprene organonitrates on the  
741 basis of their condensation behavior. Figure 6 shows how the signals of gas-phase products change in  
742 experiments with and without seed aerosols (ammonium sulfate). Please note that while the two experiments  
743 were conducted under similar conditions, the procedures could not be kept fully identical as aerosol seeding  
744 required specific measures and the oxidation chemistry might be slightly altered (e.g., due to initiation of  
745 heterogeneous reactions).

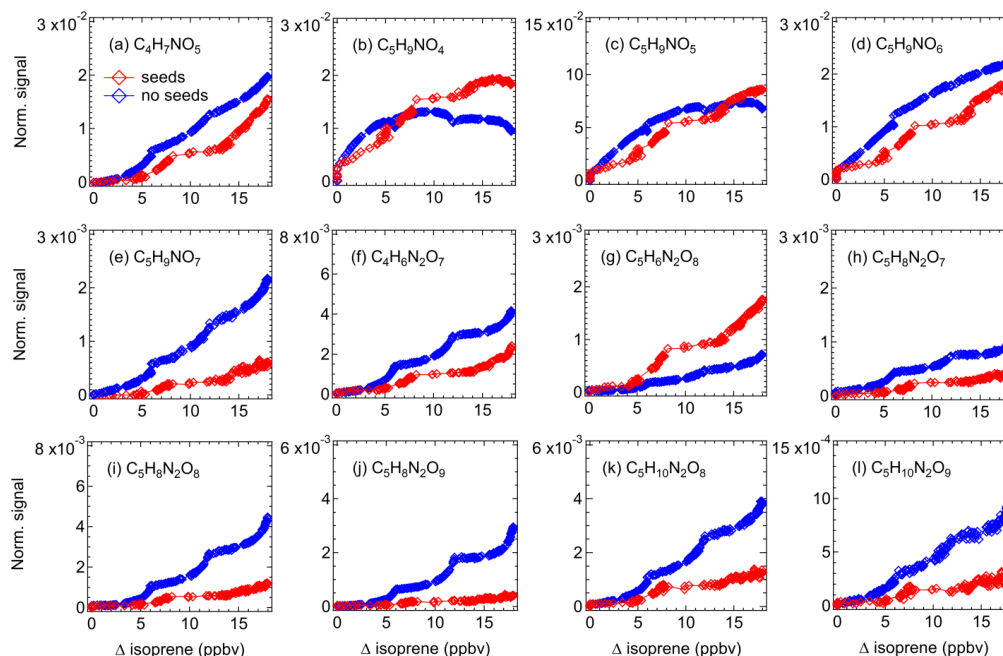
746 As shown in Fig. 6, the signals of most of the selected compounds decline when there are seed aerosols in  
747 the chamber, indicating that part of the condensable vapors is partitioned to the particle-phase due to the  
748 introduction of condensation sinks. The decrease in signal differs for different products, mostly depending on  
749 their vapor pressures. As expected, the lower volatility of a compound the higher the fraction that condenses.  
750 For instance, the signal of  $C_5H_9NO_7$  decreases by more than 70% in experiment with seed aerosols, compared to  
751 less than 40% on average for other less-oxidized 1N-monomers. In some cases (e.g.,  $C_5H_9NO_4$  and  $C_5H_9NO_5$ )  
752 however, the product signals in experiment with seed aerosols are higher than that without seeds after the  
753 consumed isoprene exceeding a certain level. In addition, the signal of  $C_5H_6N_2O_8$  in the experiment with seeds  
754 is always higher compared to that without seeds. One explanation for this phenomenon is the effect of  
755 heterogeneous reactions. It is likely that some condensed compound (denoted as A) can react on the particle  
756 surface to form new products with the molecular composition of compound B, or alternatively forming a  
757 precursor of B. When they evaporate back to the gas phase, it can result in an increase in signal of compound B.  
758 That's why a higher signal was observed for such compounds in experiment with seeds than that without seeds,  
759 as observed for  $C_5H_6N_2O_8$  in this case.

760 Based on the observed condensation behavior of different products, we can derive their vapor pressures  
761 from the gas-particle equilibrium partitioning coefficients by Eq. (2). As depicted in Fig. 7, the saturation  
762 concentrations of different organonitrates show a decreasing tendency from 1N-, 2N-monomer and 3N-  
763 monomers to 2N- and 3N-dimers, suggesting that dimers have a higher propensity of condensation and  
764 contribute to SOA formation. This is partly related to their molecular weight, as larger molecules generally have  
765 lower vapor pressures. However, it cannot explain all the features of the volatility distribution. For example,  
766  $C_5H_9NO_6$  (corresponding to No.8 in Fig.7) has higher mass than  $C_5H_9NO_5$  (corresponding to No.7 in Fig.7) but  
767 is predicted to have higher vapor pressure. In general, chemical composition and functionalities have significant  
768 effects on vapor pressure. For instance, the 2D-VBS composition-activity relationship suggests that each carbon  
769 and oxygen decrease  $C^*$  by 0.475 and 1.75 decades, respectively (Donahue et al., 2011). Different functional  
770 groups also have very different effect on volatility. For example, each hydroxyl group ( $-OH$ ) or hydroperoxy  
771 group ( $-OOH$ ) typically reduces the volatility by 2.4 to 2.5 decades, while the less polar carbonyl group ( $=O$ )  
772 reduces the volatility by 1 decade (Pankow and Asher 2008, Donahue et al., 2011). The nitrooxy group ( $-ONO_2$ )  
773 has a similar reductive effect on vapor pressure, which typically reduces  $C^*$  by 2.5 orders of magnitude (Pankow  
774 and Asher, 2008). Here, the irregularly high vapor pressure of  $C_5H_9NO_6$  is most likely attributed to the  
775 functional groups it contains. As listed in Table S2,  $C_5H_9NO_6$  is proposed to be nitrooxy hydroxy hydroperoxyl





776 compound, which consists of two highly polar functional groups –OH and –OOH, contributing to formation of  
777 intramolecular H-bonding that can significantly increase the vapor pressure (Bilde et al., 2015; Kurten et al.,  
778 2016), while  $C_5H_9NO_5$  only contains a –OOH group and hence cannot form intramolecular H-bonding. These  
779 findings underline that the constitutional and configurational information of a molecule is critical for vapor-  
780 pressure estimation.



781  
782 **Figure 6: Time evolution of selected major gas-phase products during experiments with (red) and without (blue) seed**  
783 **aerosols (ammonium sulfate). Signals have been corrected for dilution.**

### 784 3.3.2 $C^*$ estimated by different parametrization methods

785 For comparison, we also adopt different parameterization methods to estimate the saturation vapor pressures of  
786 isoprene oxidation products based on their molecular composition and the proposed structures, with the results  
787 depicted in Fig. 7. In general, the saturation concentrations calculated by different parameterization methods  
788 show a similar volatility distribution to that calculated by experimental method, with  $C^*$  of 1N-, 2N- and 3N-  
789 monomers, 2N- and 3N-dimers decreasing in turn. However, different parameterization methods lead to the  
790 predicted vapor concentrations with a variability of several orders of magnitude for the same compound, and the  
791 discrepancies become larger and larger with more complicated molecules. In addition,  $C^*$  of structural isomers  
792 calculated by the same method could span several decades.

793 As shown in Fig. 7, the Donahue et al. parameterization mostly provides lower  $C^*$  compared to the three  
794 GC methods, with a maximum discrepancy up to 12 orders of magnitude for dimers. With regard to smaller and  
795 less oxidized 1N-monomers, predicted  $C^*$  values from different methods are in relatively good agreement with  
796 each other, whereas the disagreement increases to 11 orders of magnitude for 2N- and 3N-monomers. This is  
797 mainly the case because the organic molecules were regarded as a mixture of =O and –OH functional groups in  
798 the Donahue et al. parameterization, and their relative abundance was assumed to be 1:1 (Donahue et al., 2011).



799 In consequence, the –OOH functional group in peroxides is treated as two –OH groups when adapting the  
800 method proposed by Donahue et al. (2011). However, it is demonstrated that the extra oxygen in peroxy  
801 moieties has little contribution to reduce vapor pressure (Pankow and Asher et al., 2008), hence treating –OOH  
802 equivalent to two –OH functional groups would underestimate the vapor pressures of hydroperoxyl compounds.  
803 Furthermore, organic compounds consisting of multiple polar functional groups (such as hydroperoxy, peroxy  
804 acid, and peroxide functional groups) tend to form intramolecular H-bonding, which would increase the vapor  
805 pressure (Bilde et al., 2015; Kurten et al., 2016). All these issues contribute to an underestimation of the vapor  
806 pressures of multifunctional products when using the Donahue et al. parameterization. Mohr et al. (2019)  
807 improved the parameterization for vapor-pressure estimation by taking the presence of –OOH functional groups  
808 in HOM explicitly into consideration and revising the parameters to reduce the effect of –OOH on depressing  $C^*$ .  
809 Consequently, the Mohr et al. parameterization effectively reduces the discrepancy between its estimates and  
810 those predicted by the GC methods, with the differences within 6 orders of magnitude. Nevertheless, there is a  
811 slight tendency to underestimate the vapor pressures of 3N-monomers and dimers. The Peräkylä et al.  
812 parameterization method, which was derived from measurements of the condensation behavior of HOM  
813 produced from  $\alpha$ -pinene ozonolysis, predicts similar  $C^*$  to Donahue et al. method for 1N-monomers, but higher  
814  $C^*$  for 2N- and 3N-monomers like the Mohr et al. method. As for dimers, especially for the 3N-dimers  
815 containing more multifunctional groups, the Peräkylä et al. method even predicts higher  $C^*$  than the GC  
816 methods in most cases.

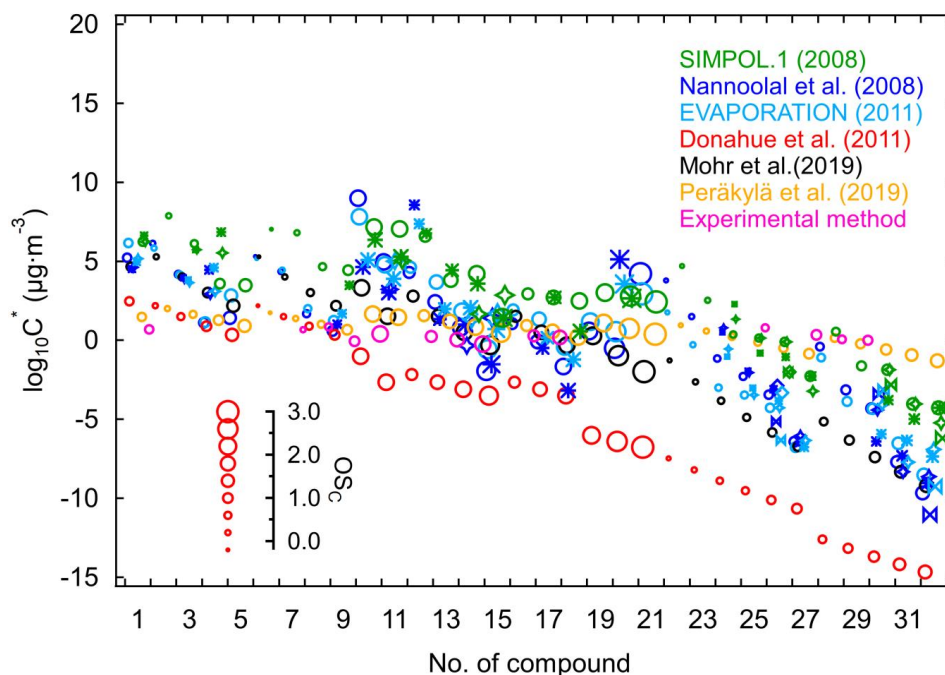
817 Three GC methods predict similar saturation vapor pressures for different isoprene nitrates in this work,  
818 with the differences within 5 orders of magnitudes. Generally, the SIMPOL.1 method always provides higher  $C^*$   
819 compared to another two methods, and the disagreement between methods becomes larger for molecules  
820 containing multifunctional groups. For instance, the vapor-pressure discrepancy between SIMPOL.1 and  
821 another two GC methods are both 2 orders of magnitude for  $C_5H_9NO_{4,5}$  and  $C_{10}H_{17}N_3O_{12-14}$ , but it increased up  
822 to 4 and 5 orders of magnitude, respectively, for  $C_5H_9NO_{6,7}$  and  $C_{10}H_{17}N_3O_{15,16}$ .

823 It is worth noting that the Nannoolal et al. method is able to distinguish between positional isomers (e.g.,  
824 the estimated  $C^*$  for two  $C_5H_{10}N_2O_9$  isomers are 0.858 and 0.333  $\mu\text{g m}^{-3}$ , respectively), whereas such capacity of  
825 EVAPORATION method is limited (e.g., it is able to distinguish between the position isomers of  $C_5H_{10}N_2O_9$ ,  
826 but it predicts identical  $C^*$  for  $C_{10}H_{16}N_2O_{11}$  isomers). In this respect, the SIMPOL.1 method cannot distinguish  
827 between positional isomers at all. Moreover, SIMPOL.1 method predicts smaller differences between functional  
828 group isomers for 1N-monomers and 3N-dimers compared to the Nannoolal et al. method and the  
829 EVAPORATION, but there is no such regular pattern for 2N-monomers and 2N-dimers.

830 By comparing the results calculated by experimental method with those by different parameterization  
831 methods, we can see that the GC methods predict lower saturation concentrations for 1N-monomers than the  
832 experimental method, while the Donahue et al. and Peräkylä et al. method provide similar  $C^*$  values. With  
833 regard to 2N-monomers, the GC methods predict higher vapor pressures compared to the experimental method,  
834 and the discrepancy decreases with decreasing saturation concentration. The disagreement of  $C^*$  for 2N-  
835 monomers estimated by experimental method and the Mohr et al. or Peräkylä et al. method are within 2 orders  
836 of magnitude. In terms of low-volatility dimers, however, the vapor pressures calculated by the experimental  
837 method were 1–3 orders of magnitude larger than that predicted by the parameterization methods except for the  
838 Peräkylä et al. method. The Peräkylä et al. method provides the most similar predictions to the experimental



839 method for isoprene oxidation products in the full volatility range, with the disagreement within 1 order of  
840 magnitude.



841  
842 **Figure 7: Saturation concentrations (in  $\mu\text{g m}^{-3}$ , at 298.15 K) of isoprene organonitrates estimated by using**  
843 **experimental and parameterization methods. The numbers correspond with the compound numbers of given in Table**  
844 **S2 (No. 1–9, 10–18, 19–21, 22–27, and 28–32 corresponding to 1N-monomers, 2N-monomers, 3N-monomer, 2N-**  
845 **dimers and 3N-dimers, respectively). Marker shapes indicate different isomers, with their size scaled by carbon**  
846 **oxidation state ( $OSc$ ).**

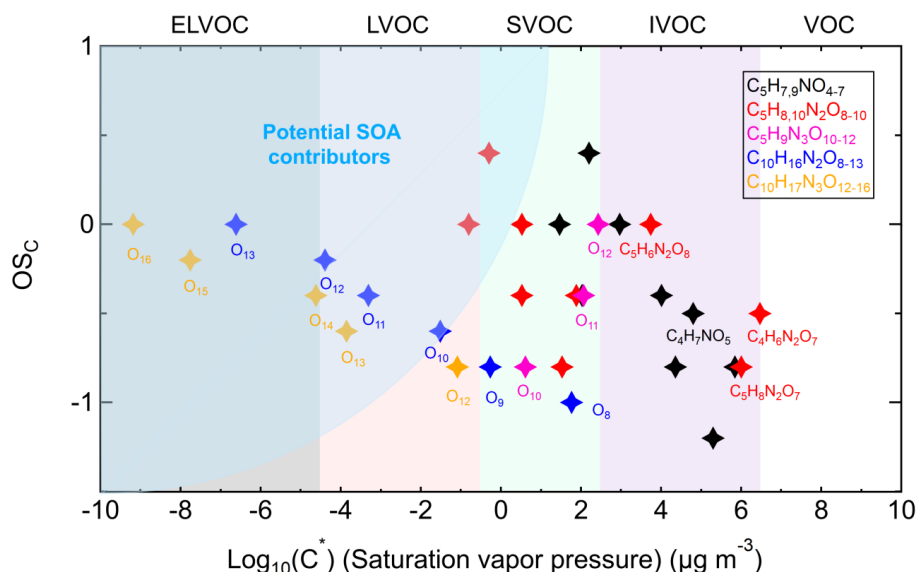
847 In general, the vapor pressures estimated experimentally in this study are very close to that calculated by  
848 Peräkylä et al. method for which the estimation parameters were also derived experimentally. The discrepancy  
849 between the experimental and the GC methods spans several orders of magnitude depending on different  
850 compounds, with the GC methods predicting lower  $C^*$  for less-functionalized 1N-monomers, approximate  $C^*$  for  
851 2N-monomers, but higher  $C^*$  for highly functionalized dimers. It is difficult to tell which method is more  
852 reliable without any measured saturation vapor pressure data on such multifunctional organic nitrates. However,  
853 considering the fact that the existing GC methods tend to underestimate saturation vapor pressures of the highly  
854 functionalized organic molecules due to their limited capability to deal with intramolecular interactions (e.g. the  
855 intramolecular hydrogen bonding formed among polar functional groups), and the well consistent results of two  
856 experimentally derived methods, we suggest that the experimental method might be a good choice to determine  
857 the volatility of highly oxidized compounds accurately.

### 858 3.3.3 Volatility distribution of isoprene nitrates and expected SOA yields.

859 Although the vapor pressures calculated by different methods show a variability of several orders of magnitude,  
860 the predicted volatility distributions of different organic groups are consistent. To eliminate the discrepancy  
861 caused by methods and get an average trend of the volatility distribution of various isoprene nitrates, we use the



862 median value of  $C^*$  calculated by different methods as the estimator of the vapor pressure for each nitrate  
863 compound.



864  
865 **Figure 8: Volatility distribution of different organonitrates formed from  $\text{NO}_3$ -initiated isoprene oxidation. The**  
866 **volatility classes are indicated along the top with corresponding colors in the plot. The position of potential SOA**  
867 **contributors is determined depending on the exact functionalities of molecules adapted from Bianchi et al. (2019).**

868 The average carbon oxidation state is plotted against  $\text{Log}_{10}(C^*)$  in Fig. 8 to describe the volatility  
869 distribution of organic nitrates formed from isoprene oxidation by  $\text{NO}_3$ . Generally, the volatility of measured  
870 gas-phase products spans a wide range from IVOC to ELVOC, wherein all of the 1N-monomers fall in the  
871 IVOC or SVOC range, suggesting that 1N-monomers have low potential to form SOA by simple condensation  
872 as long as the organic aerosol load is less than  $200 \mu\text{g m}^{-3}$ . The addition of a second or third  $-\text{NO}_3$  functional  
873 group decreases  $C^*$  of most 2N- and 3N-monomers by 2-3 decades compared with 1N-monomers, and most of  
874 them belong to SVOC. They will start to condense in significant fractions if the organic aerosol load is in a  
875 range of  $1\text{-}10 \mu\text{g m}^{-3}$ , which means 2N- and 3N-monomers with  $\text{OS}_c > -0.8$  may contribute to SOA formation  
876 under atmospheric conditions. With regard to dimers, all 3N-dimers and 2N-dimers (except for  $\text{C}_{10}\text{H}_{16}\text{N}_2\text{O}_{8,9}$ )  
877 are in LVOC or even ELVOC range, indicating isoprene dimers had high propensity to form SOA even at  
878 organic aerosol loads  $\ll 1 \mu\text{g/m}^3$ . However, we would like to emphasize here that the signals of 2N- and 3N-  
879 dimers only account for less than 2% on average of the total assigned signals, as shown in Fig. S5. This suggests  
880 that the SOA yield of isoprene from  $\text{NO}_3$  oxidation by condensation should be low under atmospheric  
881 conditions.

882 Assuming that the dimers in the LVOC or ELVOC range will condense onto particles, we estimated a SOA  
883 mass yield for condensation of isoprene organic nitrates of about 5 %. This value is based on an averaged bulk  
884 organonitrate sensitivity of  $0.019 \text{ norm. count s}^{-1} \text{ ppbv}^{-1}$  and has been corrected for wall loss and dilution (see  
885 Fig. S6, with uncorrected SOA mass yield of about 2 %). The estimated SOA mass yield is within the range of  
886 those reported in the literature, but at the lower end (4.3% to 23.8% depending on  $\text{RO}_2$  fate, Ng et al., 2008; 0.7%  
887 for first generation oxidation and 14% after oxidation of both double bonds, Rollins et al., 2009; 27% on



888 average for ambient measurements, Fry et al., 2018). The SOA yield will probably become somewhat higher if  
889 taking the contribution of the minor dimer products as well as SVOCs into consideration. Our finding is  
890 commensurable with the SOA yield for isoprene organic nitrates of 2-6% derived from HR-AMS measurements  
891 in the same campaign (Brownwood et al., in preparation).

892 In addition, Br<sup>-</sup> adduct ionization CIMS is selective for HO<sub>2</sub> and less oxidized organic compounds  
893 (Albrecht et al., 2019; Rissanen et al., 2019), so it is reasonable to assume that there were more highly oxidized  
894 products that were not detected by Br<sup>-</sup> CIMS. This assumption is confirmed by measurements with a NO<sub>3</sub><sup>-</sup> CIMS  
895 performed in another isoprene-NO<sub>3</sub> experiment in SAPHIR (Zhao et al., in preparation). Zhao et al. observed a  
896 higher fraction of dimers and more highly oxidized monomers and dimers, as well as trimers (C<sub>15</sub> compounds).  
897 As a consequence, the SOA yields derived from NO<sub>3</sub><sup>-</sup> CIMS measurements is slightly higher.

898 From these points of view our yield is more a lower limit. However, even if we assume an error of a factor  
899 of 2, the SOA yield of isoprene organic nitrates by condensation is more likely in a range of about 10% or less  
900 than in the higher range of 20-30% published in the literature. Of course, by our method we cannot cover any  
901 liquid phase processes that would lead to additional SOA beyond the condensation of the target compounds.

#### 902 **4. Conclusions and implication**

903 In this work, a gas-phase experiment conducted in the SAPHIR chamber under near atmospheric conditions in  
904 the dark was analyzed to primarily investigate the multi-generation chemistry of isoprene-NO<sub>3</sub> system. The  
905 characteristics of a diversity of isoprene nitrates were measured by the CIMS using Br<sup>-</sup> as the reagent ion.  
906 Isoprene 1N-, 2N-, and 3N-monomers and 2N- and 3N-dimers have different time behaviors, indicating the  
907 occurrence of multi-generation oxidation during this process. Based on their specific time behaviors as well as  
908 the general knowledge of isoprene and radical chemistry, the possible formation mechanisms of these  
909 compounds are proposed.

910 In order to evaluate the potential contribution of various isoprene nitrates to SOA formation, different  
911 composition-activity and group-contribution methods were used to estimate their saturation vapor pressures. We  
912 also calculated the vapor pressures of isoprene oxidation products based on the gas-particle equilibrium  
913 coefficients derived from condensation measurements. The vapor pressures estimated by different methods  
914 spans several orders of magnitude, and the discrepancies increase as the compounds become highly  
915 functionalized. It shows that existing group-contribution methods tend to underestimate the saturation vapor  
916 pressure of the multifunctional low-volatility molecules, and we suggest that experimental methods might be a  
917 good choice to estimate the volatility of highly oxidized compounds accurately.

918 According to our results, 1N-monomers and most 2N and 3N-nitrates fall in the IVOC or SVOC range.  
919 Therefore, they have, with a few exceptions, low potential to form SOA at atmospheric organic aerosol loads. In  
920 contrast, 2N- and 3N-dimers are estimated to have low or extremely low volatility, indicating that they are  
921 significant contributors to SOA formation, although dimers constitute less than 2% of the total explained signals.  
922 In this study, no new particle formation events were observed. Assuming that the dimers in the LVOC or  
923 ELVOC range will condense onto particles completely, we estimate a SOA mass yield of about 5 %, which is a  
924 lower limit if one takes a possible contribution of the minor dimer products as well as SVOC species into  
925 consideration. Both the volatility distribution and calculated SOA yields indicate that isoprene dimers formed  
926 from NO<sub>3</sub> oxidation are the major contributors to SOA formation.



927 **Data availability**

928 All data given in figures can be displayed in tables or in digital form. This includes the data given in the  
929 Supplement. The data will be made available via the repository Jülich DATA. Please send all requests for data  
930 to [t.mentel@fz-juelich.de](mailto:t.mentel@fz-juelich.de) and [r.wu@fz-juelich.de](mailto:r.wu@fz-juelich.de).

931 **Author contributions**

932 HF, JNC, JLF, SSB, AW, and AKS designed the study. Instrument deployment and data analysis were carried out  
933 by RW, ET, SK, SRA, LH, AN, HF, RT, TH, PTMC, JS, FB, BB, JAT. RW, LV, ET, DZ, JAT, MH, TFM interpreted the  
934 compiled data set. RW, TFM, LV wrote the manuscript. All co-authors discussed the results and commented on  
935 the manuscript.  
936

937 **Competing interests**

938 The authors declare that they have no conflict of interest.

939 **Acknowledgements**

940 This work has received funding from the European Research Council (ERC) and European Commission (EC)  
941 under the European Union's Horizon 2020 research and innovation program (SARLEP grant agreement No.  
942 681529, and Eurochamp 2020 grant agreement No. 730997). R.Wu gratefully acknowledges the fellowship from  
943 Helmholtz-OCPC (Office of China Postdoc Council) Postdoc Program for research support. M. Hallquist.,  
944 Th.F.Mentel. and E.Tsiligiannis gratefully acknowledge the support by the Svenska Vetenskapsrådet (grant nos.  
945 2014-05332 and 2018-04430) and the Svenska Forskningsrådet Formas (grant no. 2015-1537).

946 **References**

- 947 Albrecht, S. R., Novelli, A., Hofzumahaus, A., Kang, S., Baker, Y., Mentel, T., Wahner, A., and Fuchs, H.:  
948 Measurements of hydroperoxy radicals (HO<sub>2</sub>) at atmospheric concentrations using bromide chemical  
949 ionisation mass spectrometry, *Atmos. Meas. Tech.*, 12, 891-902, 10.5194/amt-12-891-2019, 2019.
- 950 Anglada, J. M., Crehuet, R., and Francisco, J. S.: The Stability of  $\alpha$ -Hydroperoxyalkyl Radicals, *Chem. Eur. J.*,  
951 22, 18092-18100, 2016.
- 952 Atkinson, R., and Arey, J.: Gas-phase tropospheric chemistry of biogenic volatile organic compounds: a review,  
953 *Atmos. Environ.*, 37, 197-219, 10.1016/S1352-2310(03)00391-1, 2003.
- 954 Atkinson, R.: Gas-phase tropospheric chemistry of organic compounds: a review, *Atmos. Environ.*, 41, 200-240,  
955 10.1016/j.atmosenv.2007.10.068, 2007.
- 956 Barber, V. P., Pandit, S., Green, A. M., Trongsiwat, N., Walsh, P. J., Klippenstein, S. J., and Lester, M. I.:  
957 Four-carbon Criegee intermediate from isoprene ozonolysis: Methyl vinyl ketone oxide synthesis, infrared  
958 spectrum, and OH production, *J. Am. Chem. Soc.*, 140, 10866-10880, 2018.



- 959 Berndt, T., Mentler, B., Scholz, W., Fischer, L., Herrmann, H., Kulmala, M., and Hansel, A.: Accretion Product  
960 Formation from Ozonolysis and OH Radical Reaction of alpha-Pinene: Mechanistic Insight and the  
961 Influence of Isoprene and Ethylene, *Environ. Sci. Technol.*, 52, 11069-11077, 10.1021/acs.est.8b02210,  
962 2018.
- 963 Bianchi, F., Kurten, T., Riva, M., Mohr, C., Rissanen, M. P., Roldin, P., Berndt, T., Crouse, J. D., Wennberg, P.  
964 O., Mentel, T. F., Wildt, J., Junninen, H., Jokinen, T., Kulmala, M., Worsnop, D. R., Thornton, J. A.,  
965 Donahue, N., Kjaergaard, H. G., and Ehn, M.: Highly Oxygenated Organic Molecules (HOM) from Gas-  
966 Phase Autoxidation Involving Peroxy Radicals: A Key Contributor to Atmospheric Aerosol, *Chem. Rev.*,  
967 119, 3472-3509, 10.1021/acs.chemrev.8b00395, 2019.
- 968 Bilde, M., Barsanti, K., Booth, M., Cappa, C. D., Donahue, N. M., Emanuelsson, E. U., McFiggans, G., Krieger,  
969 U. K., Marcolli, C., Topping, D., Ziemann, P., Barley, M., Clegg, S., Dennis-Smith, B., Hallquist, M.,  
970 Hallquist, A. M., Khlystov, A., Kulmala, M., Mogensen, D., Percival, C. J., Pope, F., Reid, J. P., Ribeiro da  
971 Silva, M. A., Rosenoern, T., Salo, K., Soonsin, V. P., Yli-Juuti, T., Prisle, N. L., Pagels, J., Rarey, J.,  
972 Zardini, A. A., and Riipinen, I.: Saturation vapor pressures and transition enthalpies of low-volatility  
973 organic molecules of atmospheric relevance: from dicarboxylic acids to complex mixtures, *Chem. Rev.*,  
974 115, 4115-4156, 10.1021/cr5005502, 2015.
- 975 Brown, S., Degouw, J., Warneke, C., Ryerson, T., Dubé, W., Atlas, E., Weber, R., Peltier, R., Neuman, J., and  
976 Roberts, J.: Nocturnal isoprene oxidation over the Northeast United States in summer and its impact on  
977 reactive nitrogen partitioning and secondary organic aerosol, *Atmos. Chem. Phys.*, 9, 3027-3042,  
978 10.5194/acp-9-3027-2009, 2009.
- 979 Carlton, A. G., Wiedinmyer, C., and Kroll, J. H.: A review of Secondary Organic Aerosol (SOA) formation  
980 from isoprene, *Atmos. Chem. Phys.*, 9, 4987-5005, 10.5194/acp-9-4987-2009, 2009.
- 981 Compernelle, S., Ceulemans, K., and Müller, J. F.: EVAPORATION: a new vapour pressure estimation  
982 method for organic molecules including non-additivity and intramolecular interactions, *Atmos. Chem. Phys.*,  
983 11, 9431-9450, 10.5194/acp-11-9431-2011, 2011.
- 984 Crosson, E.: A cavity ring-down analyzer for measuring atmospheric levels of methane, carbon dioxide, and  
985 water vapor, *Appl. Phys. B*, 92, 403-408, 10.1007/s00340-008-3135-y, 2008.
- 986 Crouse, J. D., Nielsen, L. B., Jørgensen, S., Kjaergaard, H. G., and Wennberg, P. O.: Autoxidation of Organic  
987 Compounds in the Atmosphere, *J. Phys. Chem. Lett.*, 4, 3513-3520, 10.1021/jz4019207, 2013.
- 988 Donahue, N. M., Robinson, A. L., Stanier, C. O., and Pandis, S. N.: Coupled partitioning, dilution, and chemical  
989 aging of semivolatile organics, *Environ. Sci. Technol.*, 40, 2635-2643, 10.1021/es052297c, 2006.
- 990 Donahue, N. M., Epstein, S. A., Pandis, S. N., and Robinson, A. L.: A two-dimensional volatility basis set: 1.  
991 organic-aerosol mixing thermodynamics, *Atmos. Chem. Phys.*, 11, 3303-3318, 10.5194/acp-11-3303-2011,  
992 2011.
- 993 Donahue, N. M., Kroll, J. H., Pandis, S. N., and Robinson, A. L.: A two-dimensional volatility basis set – Part 2:  
994 Diagnostics of organic-aerosol evolution, *Atmos. Chem. Phys.*, 12, 615-634, 10.5194/acp-12-615-2012,  
995 2012.
- 996 Dubé, W. P., Brown, S. S., Osthoff, H. D., Nunley, M. R., Ciciora, S. J., Paris, M. W., McLaughlin, R. J., and  
997 Ravishankara, A.: Aircraft instrument for simultaneous, in situ measurement of NO<sub>3</sub> and N<sub>2</sub>O<sub>5</sub> via  
998 pulsed cavity ring-down spectroscopy, *Rev. Sci. Instrum.*, 77, 034101, 10.1063/1.2176058, 2006.



- 999 Ehn, M., Thornton, J. A., Kleist, E., Sipila, M., Junninen, H., Pullinen, I., Springer, M., Rubach, F., Tillmann, R.,  
1000 Lee, B., Lopez-Hilfiker, F., Andres, S., Acir, I. H., Rissanen, M., Jokinen, T., Schobesberger, S.,  
1001 Kangasluoma, J., Kontkanen, J., Nieminen, T., Kurten, T., Nielsen, L. B., Jorgensen, S., Kjaergaard, H. G.,  
1002 Canagaratna, M., Maso, M. D., Berndt, T., Petaja, T., Wahner, A., Kerminen, V. M., Kulmala, M.,  
1003 Worsnop, D. R., Wildt, J., and Mentel, T. F.: A large source of low-volatility secondary organic aerosol,  
1004 Nature, 506, 476-479, 10.1038/nature13032, 2014.
- 1005 Friedman, B., and Farmer, D. K.: SOA and gas phase organic acid yields from the sequential photooxidation of  
1006 seven monoterpenes, Atmos. Environ., 187, 335-345, 10.1016/j.atmosenv.2018.06.003, 2018.
- 1007 Fry, J. L., Brown, S. S., Middlebrook, A. M., Edwards, P. M., Campuzano-Jost, P., Day, D. A., Jimenez, J. L.,  
1008 Allen, H. M., Ryerson, T. B., Pollack, I., Graus, M., Warneke, C., de Gouw, J. A., Brock, C. A., Gilman, J.,  
1009 Lerner, B. M., Dubé, W. P., Liao, J., and Welti, A.: Secondary organic aerosol (SOA) yields from  
1010 NO<sub>3</sub> radical + isoprene based on nighttime aircraft power plant plume transects, Atmos.  
1011 Chem. Phys., 18, 11663-11682, 10.5194/acp-18-11663-2018, 2018.
- 1012 Guenther, A., Jiang, X., Heald, C., Sakulyanontvittaya, T., Duhl, T., Emmons, L., and Wang, X.: The Model of  
1013 Emissions of Gases and Aerosols from Nature version 2.1 (MEGAN2. 1): an extended and updated  
1014 framework for modeling biogenic emissions, Geosci. Model Dev., 5, 1471-1492, 10.5194/gmd-5-1471-  
1015 2012, 2012. .
- 1016 Hallquist, M., Wenger, J., Baltensperger, U., Rudich, Y., Simpson, D., Claeys, M., Dommen, J., Donahue, N.,  
1017 George, C., and Goldstein, A.: The formation, properties and impact of secondary organic aerosol: current  
1018 and emerging issues, Atmos. Chem. Phys., 9, 5155-5236, 10.5194/acp-9-5155-2009, 2009 .
- 1019 Hu, J., Wu, L., Zheng, B., Zhang, Q., He, K., Chang, Q., Li, X., Yang, F., Ying, Q., and Zhang, H.: Source  
1020 contributions and regional transport of primary particulate matter in China, Environ. Pollut., 207, 31-42,  
1021 10.1016/j.envpol.2015.08.037, 2015.
- 1022 Jenkin, M., Young, J., and Rickard, A.: The MCM v3. 3.1 degradation scheme for isoprene, Atmos. Chem.  
1023 Phys., 15, 11433-11459, 10.5194/acp-15-11433-2015, 2015.
- 1024 Jimenez, J. L., Canagaratna, M., Donahue, N., Prevot, A., Zhang, Q., Kroll, J. H., DeCarlo, P. F., Allan, J. D.,  
1025 Coe, H., and Ng, N.: Evolution of organic aerosols in the atmosphere, science, 326, 1525-1529,  
1026 10.1126/science.1180353, 2009.
- 1027 Kim, P. S., Jacob, D. J., Fisher, J. A., Travis, K., Yu, K., Zhu, L., Yantosca, R. M., Sulprizio, M. P., Jimenez, J.  
1028 L., Campuzano-Jost, P., Froyd, K. D., Liao, J., Hair, J. W., Fenn, M. A., Butler, C. F., Wagner, N. L.,  
1029 Gordon, T. D., Welti, A., Wennberg, P. O., Crouse, J. D., St. Clair, J. M., Teng, A. P., Millet, D. B.,  
1030 Schwarz, J. P., Markovic, M. Z., and Perring, A. E.: Sources, seasonality, and trends of southeast US  
1031 aerosol: an integrated analysis of surface, aircraft, and satellite observations with the GEOS-Chem  
1032 chemical transport model, Atmos. Chem. Phys., 15, 10411-10433, 10.5194/acp-15-10411-2015, 2015.
- 1033 Kirkby, J., Duplissy, J., Sengupta, K., Frege, C., Gordon, H., Williamson, C., Heinritzi, M., Simon, M., Yan, C.,  
1034 Almeida, J., Trostl, J., Nieminen, T., Ortega, I. K., Wagner, R., Adamov, A., Amorim, A., Bernhammer, A.  
1035 K., Bianchi, F., Breitenlechner, M., Brilke, S., Chen, X., Craven, J., Dias, A., Ehrhart, S., Flagan, R. C.,  
1036 Franchin, A., Fuchs, C., Guida, R., Hakala, J., Hoyle, C. R., Jokinen, T., Junninen, H., Kangasluoma, J.,  
1037 Kim, J., Krapf, M., Kurten, A., Laaksonen, A., Lehtipalo, K., Makhmutov, V., Mathot, S., Molteni, U.,  
1038 Onnela, A., Perakyla, O., Piel, F., Petaja, T., Praplan, A. P., Pringle, K., Rap, A., Richards, N. A., Riipinen,





- 1039 I., Rissanen, M. P., Rondo, L., Sarnela, N., Schobesberger, S., Scott, C. E., Seinfeld, J. H., Sipila, M.,  
1040 Steiner, G., Stozhkov, Y., Stratmann, F., Tome, A., Virtanen, A., Vogel, A. L., Wagner, A. C., Wagner, P.  
1041 E., Weingartner, E., Wimmer, D., Winkler, P. M., Ye, P., Zhang, X., Hansel, A., Dommen, J., Donahue, N.  
1042 M., Worsnop, D. R., Baltensperger, U., Kulmala, M., Carslaw, K. S., and Curtius, J.: Ion-induced  
1043 nucleation of pure biogenic particles, *Nature*, 533, 521-526, 10.1038/nature17953, 2016.
- 1044 Kleindienst, T. E., Lewandowski, M., Offenberg, J. H., Jaoui, M., and Edney, E. O.: Ozone-isoprene reaction:  
1045 Re-examination of the formation of secondary organic aerosol, *Geophys. Res. Lett.*, 34,  
1046 10.1029/2006GL027485, 2007.
- 1047 Krechmer, J., Lopez-Hilfiker, F., Koss, A., Hutterli, M., Stoermer, C., Deming, B., Kimmel, J., Warneke, C.,  
1048 Holzinger, R., Jayne, J., Worsnop, D., Fuhrer, K., Gonin, M., and de Gouw, J.: Evaluation of a New  
1049 Reagent-Ion Source and Focusing Ion-Molecule Reactor for Use in Proton-Transfer-Reaction Mass  
1050 Spectrometry, *Anal. Chem.*, 90, 12011-12018, 10.1021/acs.analchem.8b02641, 2018.
- 1051 Kroll, J. H., Ng, N. L., Murphy, S. M., Flagan, R. C., and Seinfeld, J. H.: Secondary organic aerosol formation  
1052 from isoprene photooxidation, *Environ. Sci. Technol.*, 40, 1869-1877, 10.1021/es0524301, 2006.
- 1053 Kroll, J. H., Donahue, N. M., Jimenez, J. L., Kessler, S. H., Canagaratna, M. R., Wilson, K. R., Altieri, K. E.,  
1054 Mazzoleni, L. R., Wozniak, A. S., Bluhm, H., Mysak, E. R., Smith, J. D., Kolb, C. E., and Worsnop, D. R.:  
1055 Carbon oxidation state as a metric for describing the chemistry of atmospheric organic aerosol, *Nat. Chem.*,  
1056 3, 133-139, 10.1038/nchem.948, 2011.
- 1057 Kurten, T., Tiunanen, K., Roldin, P., Rissanen, M., Luy, J.-N., Boy, M., Ehn, M., and Donahue, N.:  $\alpha$ -Pinene  
1058 autoxidation products may not have extremely low saturation vapor pressures despite high O: C ratios, *J.*  
1059 *Phys. Chem. A*, 120, 2569-2582, 10.1021/acs.jpca.6b02196, 2016.
- 1060 Kwan, A., Chan, A., Ng, N., Kjærgaard, H. G., Seinfeld, J., and Wennberg, P.: Peroxy radical chemistry and OH  
1061 radical production during the NO<sub>3</sub>-initiated oxidation of isoprene, *Atmos. Chem. Phys.*, 12, 7499-7515,  
1062 10.5194/acp-12-7499-2012, 2012.
- 1063 Marais, E. A., Jacob, D. J., Jimenez, J. L., Campuzano-Jost, P., Day, D. A., Hu, W., Krechmer, J., Zhu, L., Kim,  
1064 P. S., Miller, C. C., Fisher, J. A., Travis, K., Yu, K., Hanisco, T. F., Wolfe, G. M., Arkinson, H. L., Pye, H.  
1065 O. T., Froyd, K. D., Liao, J., and McNeill, V. F.: Aqueous-phase mechanism for secondary organic aerosol  
1066 formation from isoprene: application to the southeast United States and co-benefit of SO<sub>2</sub> emission  
1067 controls, *Atmos. Chem. Phys.*, 16, 1603-1618, 10.5194/acp-16-1603-2016, 2016.
- 1068 McFiggans, G., Mentel, T. F., Wildt, J. r., Pullinen, I., Kang, S., Kleist, E., Schmitt, S., Springer, M., Tillmann,  
1069 R., Wu, C., Zhao, D., Hallquist, M., Faxon, C., Le Breton, M., Hallquist, A. s. M., Simpson, D., Bergström,  
1070 R., Jenkin, M. E., Ehn, M., Thornton, J. A., Alfarra, M. R., Bannan, T. J., Percival, C. J., Priestley, M.,  
1071 Topping, D., and Kiendler-Scharr, A.: Secondary organic aerosol reduced by mixture of atmospheric  
1072 vapours, *Nature*, 565, 587-593, 10.1038/s41586-018-0871-y, 2019.
- 1073 Mentel, T. F., Springer, M., Ehn, M., Kleist, E., Pullinen, I., Kurtén, T., Rissanen, M., Wahner, A., and Wildt, J.:  
1074 Formation of highly oxidized multifunctional compounds: autoxidation of peroxy radicals formed in the  
1075 ozonolysis of alkenes – deduced from structure–product relationships, *Atmos. Chem. Phys.*, 15, 6745-6765,  
1076 10.5194/acp-15-6745-2015, 2015.



- 1077 Mohr, C., Thornton, J. A., Heitto, A., Lopez-Hilfiker, F. D., Lutz, A., Riipinen, I., Hong, J., Donahue, N. M.,  
1078 Hallquist, M., Petaja, T., Kulmala, M., and Yli-Juuti, T.: Molecular identification of organic vapors driving  
1079 atmospheric nanoparticle growth, *Nat. Commun.*, 10, 4442, 10.1038/s41467-019-12473-2, 2019.
- 1080 Molteni, U., Simon, M., Heinritzi, M., Hoyle, C. R., Bernhammer, A.-K., Bianchi, F., Breitenlechner, M., Brilke,  
1081 S., Dias, A., Duplissy, J., Frege, C., Gordon, H., Heyn, C., Jokinen, T., Kürten, A., Lehtipalo, K.,  
1082 Makhmutov, V., Petäjä, T., Pieber, S. M., Praplan, A. P., Schobesberger, S., Steiner, G., Stozhkov, Y.,  
1083 Tomé, A., Tröstl, J., Wagner, A. C., Wagner, R., Williamson, C., Yan, C., Baltensperger, U., Curtius, J.,  
1084 Donahue, N. M., Hansel, A., Kirkby, J., Kulmala, M., Worsnop, D. R., and Dommen, J.: Formation of  
1085 Highly Oxygenated Organic Molecules from  $\alpha$ -Pinene Ozonolysis: Chemical Characteristics, Mechanism,  
1086 and Kinetic Model Development, *ACS Earth Space Chem.*, 3, 873-883,  
1087 10.1021/acsearthspacechem.9b00035, 2019.
- 1088 Mutzel, A., Rodigast, M., Iinuma, Y., Böge, O., and Herrmann, H.: Monoterpene SOA – Contribution of first-  
1089 generation oxidation products to formation and chemical composition, *Atmos. Environ.*, 130, 136-144,  
1090 10.1016/j.atmosenv.2015.10.080, 2016.
- 1091 Nannoolal, Y., Rarey, J., Ramjugernath, D., and Cordes, W.: Estimation of pure component properties: Part 1.  
1092 Estimation of the normal boiling point of non-electrolyte organic compounds via group contributions and  
1093 group interactions, *Fluid Phase Equilib.*, 226, 45-63, 10.1016/j.fluid.2004.09.001, 2004.
- 1094 Nannoolal, Y., Rarey, J., and Ramjugernath, D.: Estimation of pure component properties: Part 3. Estimation of  
1095 the vapor pressure of non-electrolyte organic compounds via group contributions and group interactions,  
1096 *Fluid Phase Equilib.*, 269, 117-133, 10.1016/j.fluid.2008.04.020, 2008.
- 1097 Ng, N., Kwan, A., Surratt, J., Chan, A., Chhabra, P., Sorooshian, A., Pye, H. O., Crouse, J., Wennberg, P., and  
1098 Flagan, R.: Secondary organic aerosol (SOA) formation from reaction of isoprene with nitrate radicals  
1099 ( $\text{NO}_3$ ), *Atmos. Chem. Phys.*, 8, 4117–4140, 10.5194/acp-8-4117-2008, 2008.
- 1100 Ng, N. L., Chhabra, P. S., Chan, A. W. H., Surratt, J. D., Kroll, J. H., Kwan, A. J., McCabe, D. C., Wennberg, P.  
1101 O., Sorooshian, A., Murphy, S. M., Dalleska, N. F., Flagan, R. C., and Seinfeld, J. H.: Effect of  
1102  $\text{NO}_x$  level on secondary organic aerosol (SOA) formation from the photooxidation of terpenes,  
1103 *Atmos. Chem. Phys.*, 7, 5159-5174, 10.5194/acp-7-5159-2007, 2007.
- 1104 Ng, N. L., Brown, S. S., Archibald, A. T., Atlas, E., Cohen, R. C., Crowley, J. N., Day, D. A., Donahue, N. M.,  
1105 Fry, J. L., Fuchs, H., Griffin, R. J., Guzman, M. I., Herrmann, H., Hodzic, A., Iinuma, Y., Jimenez, J. L.,  
1106 Kiendler-Scharr, A., Lee, B. H., Luecken, D. J., Mao, J., McLaren, R., Mutzel, A., Osthoff, H. D., Ouyang,  
1107 B., Picquet-Varrault, B., Platt, U., Pye, H. O. T., Rudich, Y., Schwantes, R. H., Shiraiwa, M., Stutz, J.,  
1108 Thornton, J. A., Tilgner, A., Williams, B. J., and Zaveri, R. A.: Nitrate radicals and biogenic volatile  
1109 organic compounds: oxidation, mechanisms, and organic aerosol, *Atmos. Chem. Phys.*, 17, 2103-2162,  
1110 10.5194/acp-17-2103-2017, 2017.
- 1111 Novelli, A., Vereecken, L., Bohn, B., Dorn, H.-P., Gkatzelis, G. I., Hofzumahaus, A., Holland, F., Reimer, D.,  
1112 Rohrer, F., and Rosanka, S.: Importance of isomerization reactions for OH radical regeneration from the  
1113 photo-oxidation of isoprene investigated in the atmospheric simulation chamber SAPHIR, *Atmos. Chem.*  
1114 *Phys.*, 20, 3333–3355, 10.5194/acp-20-3333-2020, 2020.
- 1115 O'Meara, S., Booth, A. M., Barley, M. H., Topping, D., and McFiggans, G.: An assessment of vapour pressure  
1116 estimation methods, *Phys. Chem. Chem. Phys.*, 16, 19453-19469, 10.1039/c4cp00857j, 2014.



- 1117 Orlando, J. J., Tyndall, G. S., and Wallington, T. J.: The atmospheric chemistry of alkoxy radicals, *Chem. Rev.*,  
1118 103, 4657–4690, 10.1021/cr020527p, 2003.
- 1119 Orlando, J. J., and Tyndall, G. S.: Laboratory studies of organic peroxy radical chemistry: an overview with  
1120 emphasis on recent issues of atmospheric significance, *Chem. Soc. Rev.*, 41, 6294–6317,  
1121 10.1039/C2CS35166H, 2012.
- 1122 Pankow, J. F., and Asher, W. E.: SIMPOL.1: a simple group contribution method for predicting vapor pressures  
1123 and enthalpies of vaporization of multifunctional organic compounds, *Atmos. Chem. Phys.*, 8, 2773–2796,  
1124 10.5194/acp-8-2773-2008, 2008.
- 1125 Peeters, J., Müller, J.-F. o., Stavrou, T., and Nguyen, V. S.: Hydroxyl radical recycling in isoprene oxidation  
1126 driven by hydrogen bonding and hydrogen tunneling: The upgraded LIM1 mechanism, *J. Phys. Chem. A*,  
1127 118, 8625–8643, 10.1021/jp5033146, 2014.
- 1128 Peräkylä, O., Riva, M., Heikkinen, L., Quéléver, L., Roldin, P., and Ehn, M.: Experimental investigation into the  
1129 volatilities of highly oxygenated organic molecules (HOM), *Atmos. Chem. Phys.*, 20, 649–669,  
1130 10.5194/acp-20-649-2020, 2020.
- 1131 Pöschl, U.: Atmospheric aerosols: composition, transformation, climate and health effects, *Angew. Chem. Int.*  
1132 *Ed.*, 44, 7520–7540, 10.1002/anie.200501122, 2005.
- 1133 Praske, E., Otkjær, R. V., Crouse, J. D., Hethcox, J. C., Stoltz, B. M., Kjaergaard, H. G., and Wennberg, P. O.:  
1134 Atmospheric autoxidation is increasingly important in urban and suburban North America, *Proc. Natl.*  
1135 *Acad. Sci. U.S.A.*, 115, 64–69, 10.1073/pnas.1715540115, 2018.
- 1136 Rissanen, M. P., Kurten, T., Sipila, M., Thornton, J. A., Kangasluoma, J., Sarnela, N., Junninen, H., Jorgensen,  
1137 S., Schallhart, S., Kajos, M. K., Taipale, R., Springer, M., Mentel, T. F., Ruuskanen, T., Petaja, T.,  
1138 Worsnop, D. R., Kjaergaard, H. G., and Ehn, M.: The formation of highly oxidized multifunctional  
1139 products in the ozonolysis of cyclohexene, *J. Am. Chem. Soc.*, 136, 15596–15606, 10.1021/ja507146s,  
1140 2014.
- 1141 Rissanen, M. P., Mikkilä, J., Iyer, S., and Hakala, J.: Multi-scheme chemical ionization inlet (MION) for fast  
1142 switching of reagent ion chemistry in atmospheric pressure chemical ionization mass spectrometry (CIMS)  
1143 applications, *Atmos. Meas. Tech.*, 12, 6635–6646, 10.5194/amt-12-6635-2019, 2019.
- 1144 Riva, M., Rantala, P., Krechmer, J. E., Peräkylä, O., Zhang, Y., Heikkinen, L., Garmash, O., Yan, C., Kulmala,  
1145 M., Worsnop, D., and Ehn, M.: Evaluating the performance of five different chemical ionization techniques  
1146 for detecting gaseous oxygenated organic species, *Atmos. Meas. Tech.*, 12, 2403–2421, 10.5194/amt-12-  
1147 2403-2019, 2019.
- 1148 Rohrer, F., Bohn, B., Brauers, T., Brüning, D., Johnen, F. J., Wahner, A., and Kleffmann, J.: Characterisation of  
1149 the photolytic HONO-source in the atmosphere simulation chamber SAPHIR, *Atmos. Chem. Phys.*, 5,  
1150 2189–2201, 10.5194/acp-5-2189-2005, 2005.
- 1151 Rollins, A. W., Kiendler-Scharr, A., Fry, J., Brauers, T., Brown, S. S., Dorn, H.-P., Dubé, W. P., Fuchs, H.,  
1152 Mensah, A., and Mentel, T.: Isoprene oxidation by nitrate radical: alkyl nitrate and secondary organic  
1153 aerosol yields, *Atmos. Chem. Phys.*, 9, 6685–6703, 10.5194/acp-9-6685-2009, 2009.
- 1154 Schwantes, R. H., Teng, A. P., Nguyen, T. B., Coggon, M. M., Crouse, J. D., St Clair, J. M., Zhang, X.,  
1155 Schilling, K. A., Seinfeld, J. H., and Wennberg, P. O.: Isoprene NO<sub>3</sub> Oxidation Products from the RO<sub>2</sub> +  
1156 HO<sub>2</sub> Pathway, *J. Phys. Chem. A*, 119, 10158–10171, 10.1021/acs.jpca.5b06355, 2015.



- 1157 Schwantes, R. H., Charan, S. M., Bates, K. H., Huang, Y., Nguyen, T. B., Mai, H., Kong, W., Flagan, R. C., and  
1158 Seinfeld, J. H.: Low-volatility compounds contribute significantly to isoprene secondary organic aerosol  
1159 (SOA) under high-NO<sub>2</sub> conditions, *Atmos. Chem. Phys.*, 19,  
1160 7255-7278, 10.5194/acp-19-7255-2019, 2019.
- 1161 Sobanski, N., Schuladen, J., Schuster, G., Lelieveld, J., and Crowley, J. N.: A five-channel cavity ring-down  
1162 spectrometer for the detection of NO<sub>2</sub>, NO<sub>3</sub>, N<sub>2</sub>O<sub>5</sub>, total peroxy nitrates and total alkyl nitrates, *Atmos.*  
1163 *Meas. Tech.*, 9, 5103–5118, 10.5194/amt-9-5103-2016, 2016.
- 1164 Spracklen, D., Jimenez, J., Carslaw, K., Worsnop, D., Evans, M., Mann, G., Zhang, Q., Canagaratna, M., Allan,  
1165 J., and Coe, H.: Aerosol mass spectrometer constraint on the global secondary organic aerosol budget,  
1166 *Atmos. Chem. Phys.*, 11, 12109–12136, 10.5194/acp-11-12109-2011, 2011.
- 1167 Stadtler, S., Kühn, T., Schröder, S., Taraborrelli, D., Schultz, M. G., and Kokkola, H.: Isoprene-derived  
1168 secondary organic aerosol in the global aerosol–chemistry–climate model ECHAM6.3.0–HAM2.3–  
1169 MOZI.0, *Geosci. Model Dev.*, 11, 3235-3260, 10.5194/gmd-11-3235-2018, 2018.
- 1170 Suh, I., Lei, W., and Zhang, R.: Experimental and Theoretical Studies of Isoprene Reaction with NO<sub>3</sub>, *J. Phys.*  
1171 *Chem. A*, 105, 6471-6478, 10.1021/jp0105950, 2001.
- 1172 Surratt, J. D., Chan, A. W., Eddingsaas, N. C., Chan, M., Loza, C. L., Kwan, A. J., Hersey, S. P., Flagan, R. C.,  
1173 Wennberg, P. O., and Seinfeld, J. H.: Reactive intermediates revealed in secondary organic aerosol  
1174 formation from isoprene, *Proc. Natl. Acad. Sci. U.S.A.*, 107, 6640-6645, 10.1073/pnas.0911114107, 2010.
- 1175 Thornton, J. A., Shilling, J. E., Shrivastava, M., D’Ambro, E. L., Zawadowicz, M. A., and Liu, J.: A Near-  
1176 Explicit Mechanistic Evaluation of Isoprene Photochemical Secondary Organic Aerosol Formation and  
1177 Evolution: Simulations of Multiple Chamber Experiments with and without Added NO<sub>x</sub>, *ACS Earth Space*  
1178 *Chem.*, 10.1021/acsearthspacechem.0c00118, 2020.
- 1179 Tröstl, J., Chuang, W. K., Gordon, H., Heinritzi, M., Yan, C., Molteni, U., Ahlm, L., Frege, C., Bianchi, F., and  
1180 Wagner, R.: The role of low-volatility organic compounds in initial particle growth in the atmosphere,  
1181 *Nature*, 533, 527-531, 10.1038/nature18271, 2016.
- 1182 Vereecken, L., Nguyen, T. L., Hermans, I., and Peeters, J.: Computational study of the stability of  $\alpha$ -  
1183 hydroperoxyl-or  $\alpha$ -alkylperoxyl substituted alkyl radicals, *Chem. Phys. Lett.*, 393, 432-436,  
1184 10.1016/j.cplett.2004.06.076, 2004.
- 1185 Vereecken, L.: Computational study of the stability of  $\alpha$ -nitroxy-substituted alkyl radicals, *Chem. Phys. Lett.*,  
1186 466, 127-130, 10.1016/j.cplett.2008.10.042, 2008.
- 1187 Vereecken, L., and Peeters, J.: Decomposition of substituted alkoxy radicals—part I: a generalized structure–  
1188 activity relationship for reaction barrier heights, *Phys. Chem. Chem. Phys.*, 11, 9062-9074,  
1189 10.1039/B909712K, 2009.
- 1190 Vereecken, L., and Peeters, J.: A structure–activity relationship for the rate coefficient of H-migration in  
1191 substituted alkoxy radicals, *Phys. Chem. Chem. Phys.*, 12, 12608-12620, 10.1039/C0CP00387E, 2010.
- 1192 Vereecken, L., and Francisco, J. S.: Theoretical studies of atmospheric reaction mechanisms in the troposphere,  
1193 *Chem. Soc. Rev.*, 41, 6259-6293, 10.1039/C2CS35070J, 2012.
- 1194 Vereecken, L., and Nozière, B.: H migration in peroxy radicals under atmospheric conditions, *Atmos. Chem.*  
1195 *Phys.*, 20, 7429-7458, 10.5194/acp-20-7429-2020, 2020.



- 1196 Wang, S., Riva, M., Yan, C., Ehn, M., and Wang, L.: Primary formation of highly oxidized multifunctional  
1197 products in the OH-Initiated oxidation of Isoprene: a combined theoretical and experimental study, *Environ.*  
1198 *Sci. Technol.*, 52, 12255-12264, 10.1021/acs.est.8b02783, 2018.
- 1199 Wennberg, P. O., Bates, K. H., Crouse, J. D., Dodson, L. G., McVay, R. C., Mertens, L. A., Nguyen, T. B.,  
1200 Praske, E., Schwantes, R. H., and Smarte, M. D.: Gas-phase reactions of isoprene and its major oxidation  
1201 products, *Chem. Rev.*, 118, 3337-3390, 10.1021/acs.chemrev.7b00439, 2018.
- 1202 Whalley, L., Stone, D., and Heard, D.: New insights into the tropospheric oxidation of isoprene: combining field  
1203 measurements, laboratory studies, chemical modelling and quantum theory, in: *Atmospheric and Aerosol*  
1204 *Chemistry*, edited by: McNeill, V. F., and Ariya, P. A., Springer, Berlin, Heidelberg, Germany, 55-95,  
1205 10.1007/128\_2012\_359, 2012.
- 1206 Zhang, Q., Jimenez, J. L., Canagaratna, M., Allan, J., Coe, H., Ulbrich, I., Alfarra, M., Takami, A., Middlebrook,  
1207 A., and Sun, Y.: Ubiquity and dominance of oxygenated species in organic aerosols in anthropogenically -  
1208 influenced Northern Hemisphere midlatitudes, *Geophys. Res. Lett.*, 34, 10.1029/2007GL029979, 2007.
- 1209 Ziemann, P. J., and Atkinson, R.: Kinetics, products, and mechanisms of secondary organic aerosol formation,  
1210 *Chem. Soc. Rev.*, 41, 6582-6605, 10.1039/c2cs35122f, 2012.